

STUDY OF AQUATIC AND TRACE ELEMENT CHEMISTRY IN THE GREAT  
SALT LAKE: RESPONSE TO ENGINEERED AND HYDROLOGIC  
FORCINGS, AND TEMPORAL CORRESPONDENCE  
AMONG WATER AND BRINE SHRIMP

by

Shu Yang

A dissertation submitted to the faculty of  
The University of Utah  
in partial fulfillment of the requirements for the degree of

Doctor of Philosophy

in

Geology

Department of Geology and Geophysics

The University of Utah

May 2019

Copyright © Shu Yang 2019

All Rights Reserved

**The University of Utah Graduate School**

**STATEMENT OF DISSERTATION APPROVAL**

The dissertation of Shu Yang

has been approved by the following supervisory committee members:

William P. Johnson, Chair 12/5/2018  
Date Approved

Diego P. Fernandez, Member 12/5/2018  
Date Approved

Douglas Kip Solomon, Member 12/5/2018  
Date Approved

Gabriel J. Bowen, Member 12/5/2018  
Date Approved

Frank J. Black, Member 12/5/2018  
Date Approved

and by Thure Cerling, Chair/Dean of

the Department/College/School of Geology and Geophysics

and by David B. Kieda, Dean of The Graduate School.

## ABSTRACT

Aquatic and trace element chemistry parameters in the Great Salt Lake (GSL), Utah, USA were monitored to address the system response to density restratification. Six months following the engineered breach of the causeway separating the North and South Arms of the lake, restratification progressed from north to south, with associated sustained anoxia, robust sulfide (3-15 mg/L), elevated methyl-mercury (14-23 ng/L), and total mercury (17-55 ng/L) concentrations in deep water. These observations demonstrate that the system is reverting to its previous stratified condition wherein density stratification drove accumulation of high methyl mercury concentrations in the lake's deep brine waters (layers) (ranging 20-30 ng/L). Percent spiked inorganic mercury methylated (%<sup>204</sup>iHg) in both deep water and underlying sediments were examined to understand the role of the deep brine layer. The observed lack of significant difference of %<sup>204</sup>iHg under stratified versus destratified conditions indicated that the deep brine layer promotes accumulation (rather than generation) of methyl-mercury and total mercury at depth. Under destratified conditions, hydrologic (snowmelt runoff) forcing yielded stratification with temporal anoxia, concomitant with elevated concentrations of sulfide (2-6 mg/L), methyl-mercury (8-13 ng/L), and total mercury (20-40 ng/L) in deep water, highlighted the role of organic carbon in underlying sediment.

Frequent and co-located water and brine shrimp samples were collected for a 2-year period to investigate the transfer routes of trace elements from water to biota.

Temporal correspondence between brine shrimp and water concentrations were observed for selenium and mercury, with repeated year-to-year timing of peak concentrations for mercury but not selenium. Temporal correspondence was strong between brine shrimp and shallow filtered water, suggesting exposure of biota to both elements occurred mainly in surface water although mercury concentrations were much greater in deep water.

## TABLE OF CONTENTS

ABSTRACT.....	iii
ACKNOWLEDGMENTS .....	vii
Chapters	
1 INTRODUCTION .....	1
1.1 Background .....	1
1.1.1 Density Stratified Layering.....	1
1.1.2 Trace Elements in GSL Ecosystem.....	3
1.1.3 Role of DBL on MeHg Accumulation.....	4
1.2 Research Objectives and Outline .....	5
2 RESPONSE OF AQUATIC CHEMISTRY AND METHYL MERCURY CONCENTRATION IN GREAT SALT LAKE, UTAH, USA TO ENGINEERED AND HYDROLOGIC FORCINGS .....	7
2.1 Abstract.....	7
2.2 Introduction.....	8
2.3 Methods.....	10
2.3.1 Locations.....	10
2.3.2 Sampling and Analyses.....	11
2.4 Results.....	16
2.4.1 Engineered Destratification and Restratification .....	16
2.5 Discussion .....	20
2.5.1 Influences of Hydrologic Context.....	20
2.5.2 Combined Influences of Engineered and Hydrologic Perturbations ....	22
2.5.3 Role of Underlying Sediment .....	23
2.5.4 Role of DBL.....	24
2.5.5 Sources and Pathways.....	25
2.6 Acknowledgement .....	27
3 TEMPORAL CORRESPONDENCE AND PARTITIONING OF SELENIUM AND MERCURY AMONG BRINE SHRIMP AND WATER IN GREAT SALT LAKE, UTAH, USA .....	34
3.1 Abstract.....	34
3.2 Introduction.....	35
3.3 Method .....	38

3.3.1 Locations.....	38
3.3.2 Sampling and Analyses.....	38
3.4 Results.....	41
3.5 Discussion .....	43
3.5.1 Seasonality .....	43
3.5.2 Partitioning.....	45
3.5.3 Pathways to Biota .....	46
3.6 Acknowledgement .....	48
<b>4 CONCLUSION.....</b>	<b>54</b>
<b>Appendices</b>	
<b>A SUPPORTING INFORMATION FOR CHAPTER 2.....</b>	<b>56</b>
<b>B SUPPORTING INFORMATION FOR CHAPTER 3 .....</b>	<b>73</b>
<b>REFERENCES .....</b>	<b>89</b>

## ACKNOWLEDGMENTS

I am very thankful for all the support and guidance I have received from my graduate advisor, Bill Johnson. He led me to become a researcher, and supported me whenever I needed help during all stages of this work. Additionally, I want to thank my fellow graduate students who collaborated at various levels.

I want to thank my committee members: Dr. Diego Fernandez, Dr. Frank Black, Dr. Douglas Kip Solomon, and Dr. Grabriel Bowen, for their useful comments, discussions, and support throughout the years.

I am grateful to my husband, Liyan, for his love and for supporting me to chase my dream. I want to thank my parents for their coaching and support whenever and wherever I need them. Lastly, I would like to thank my sons; they made me a strong women and give me courage to face life, no matter how hard it will be.

## CHAPTER 1

### INTRODUCTION

#### 1.1 Background

##### 1.1.1 Density Stratified Layering

The Great Salt Lake (GSL), located in northwestern Utah, USA, is the largest terminal lake in the Western Hemisphere, and an important ecosystem for millions of migratory birds. The GSL is recognized as a site of hemispheric importance by the Western Hemisphere Shorebird Reserve Network, with over 1.4 million shorebirds using the GSL and surrounding wetlands for breeding and staging areas (Aldrich and Paul, 2002), and over seven million water birds utilizing the GSL and its associated wetlands during some portion of their biannual migration (Cline et al., 2011).

The construction of a railroad causeway in 1959 restricted flow between the North Arm (Gunnison Bay) and the South Arm (Gilbert Bay) (Loving et al., 2000). Because more than 90% of the freshwater runoff enters the South Arm of the lake, the North Arm brine is evaporatively concentrated to be more saline (16 to 29% salinity) and denser than the South Arm brine (6 to 28% salinity) (Stephens et al., 1990). Limited flow of denser North Arm brine to the South Arm produces a persistent deep brine layer (DBL) underlying the upper brine layer (UBL) in the South Arm (Loving et al., 2000; Gwynn, 2002; Naftz et al., 2008).

The DBL was not subject to annual turnover and was persistent despite wind forcing (Beisner et al., 2009), although periodic destratification events have been noted and inferred to be driven by wind-forced wave action (Naftz et al., 2008; Jones and Wurtsbaugh, 2014). The thickness of the mixolimnion (mixed layer) overlying the DBL was consistently reported as approximately 6-7 m, yielding an approximate maximum 2-3 m DBL thickness given the approximate 9 m maximum depth of the GSL (Loving et al., 2000; Gwynn, 2002; Naftz et al., 2008; Diaz et al., 2009; Johnson et al., 2015; Valdes et al., 2017).

The DBL is demonstrated by 1) high specific conductance, 2) low dissolved oxygen (DO), 3) high organic matter concentrations, 4) high sulfide concentrations, and 5) narrow temperature and pH range. The DBL is anoxic because photosynthesis is prevented by limited light penetration (Belovsky et al., 2011) and respiration of accumulated organic matter (Diaz et al., 2009; Johnson et al., 2015) derived from the UBL. High sulfide concentrations in the DBL (7 to 29 mg/L) (Gwynn, 2002; Jones and Wurtsbaugh, 2014; Johnson et al., 2015) are driven by abundance of electron donor (organic matter) and  $\text{SO}_4^{2-}$  relative to other major preferred electron acceptors ( $\text{O}^2$ ,  $\text{NO}^{3-}$ , Mn(IV), and Fe(II)). (Brandt et al. 2001; Ingvorsen and Brandt, 2002; Naftz et al., 2009). The DBL shows lesser temperature range than the UBL because it is insulated from surface temperatures. The DBL is warmer than the UBL in winter, and cooler than the UBL in summer (Beisner et al., 2009; Diaz et al., 2009).

Because limited flow between the North and South Arms supports density stratification, this layering can be eliminated by either: a) eliminating the flow; or by b) removing the barrier that prevents complete mixing. In December 2013, closure of the

last of two culverts (width = 4.6 m, depth = approximately 6 m) in the railroad causeway resulted in elimination of visible water exchange between the North and South Arms of the GSL. Within approximately 6 months of culvert closure, the South Arm water column was destratified, vertically homogeneous with oxic bottom waters free of dissolved sulfide (Valdes et al., 2017).

### 1.1.2 Trace Elements in GSL Ecosystem

Due to the Great Salt Lake being a terminal lake (no outflow), trace elements are evaporatively concentrated to extents that are governed by geochemical equilibria including oxidation-reduction, precipitation-dissolution, and sorption-desorption. The aqueous concentrations that result from these multiple equilibria can in some cases constitute potential threat to ecosystem and human health.

Methylmercury (MeHg) is a neurotoxin demonstrated to present health threat in numerous aquatic systems (Wood, 1974). Because mercury methylation is associated with sulfate reduction, characteristics of the DBL suggest the possibility of elevated MeHg in GSL bottom waters. DBL MeHg concentrations were shown to be on the order of 30 ng/L (Naftz et al., 2008; Johnson et al., 2015), with total mercury (THg) concentrations ranging from 30-90 ng/L (Naftz et al., 2008; Johnson et al., 2015; Valdes et al., 2017). At the same time period, these concentrations in UBL were relative low.

Selenium (Se) is a teratogen (embryonic mortality and deformity) with demonstrated negative impact to avian offspring in evaporatively concentrated aquatic systems (Ohlendorf, 2003). Although Se concentrations in water was reported relative low (approximately 0.5 µg/L for average of 2006 and 2007) (Diaz et al., 2009), a

statistical increase with net increase up to 0.34 µg/L (Diaz et al., 2009) was observed. However, antagonism between Se and mercury (Hg) toxicities, such that toxic effects were prevented by the elevated burdens of both elements, was implicated due to the fact that no reproductive impairment was observed in ducks (Conover and Vest, 2009; Ohlendorf et al., 2009).

Increasing Se concentration in water and elevated Hg concentrations in the DBL implicate it as a potential source of elevated contaminants in surrounding biota (Naftz et al., 2008; Vest et al., 2009; Wurtsbaugh et al., 2011; Saxton et al., 2013). Hg was speculated to be transferred from the DBL to the UBL by wind-driven mixing, and into the base of the food chain, and then to brine shrimp and brine fly that eventually serve as diet for birds (Belovsky et al., 2011; Wurtsbaugh et al., 2011; Saxton et al., 2013; Jones and Wurtsbaugh, 2014).

Elevated Hg concentrations in muscle from three GSL duck species (Cinnamon Teal, Northern Shoveler, Common Goldeneye) exceeded the EPA screening level of 0.3 mg/kg ww and resulted in a waterfowl consumption advisory (Scholl and Ball, 2005; Scholl and Ball, 2006). Elevated Se concentrations of liver in 15% of Common Goldeneyes was reported, suggesting sub-lethal toxic effects (Vest et al., 2009).

### 1.1.3 Role of DBL on MeHg Accumulation

In response to the above-described elimination of flow between the North and South Arms of the GSL, the destratification of the GSL yielded decreases THg concentrations in the deep waters of the South Arm of approximately 81%, and MeHg concentrations in deep waters decreased by roughly 86% (Valdes et al., 2017). MeHg

concentrations decreased by 77% in underlying surficial sediment whereas no change was observed in THg (Valdes et al., 2017). The removal of the DBL was speculated to allow for the more facile export of MeHg from the sediment into surface waters, which in turn facilitated the loss of MeHg from the system, such as via photo-demethylation (Black et al., 2012).

This, along with the fact that methylmercury production potential was robust in the underlying sediment relative to the DBL (Johnson et al., 2015), suggests that the DBL, when present, acts as a sort of cap that promotes the accumulation of methyl mercury in both surficial sediment and the DBL.

### 1.2 Research Objectives and Outline

In December 2016, a breach (width = 45.7 m, depth = 4.9 m) was opened under a new bridge in the railroad causeway to reestablish flow of water between the North and South Arms. This unintended regional-scale natural experiment provided a unique opportunity to monitor the GSL ecosystem response to reopening of flow in order to determine whether the system will return to preclosure conditions.

Chapter 2 addresses the evolution of the aquatic and trace element chemistry in the GSL ecosystem in response to re-opening of the causeway breach, which elucidated the potential roles of the DBL and underlying sediment in accumulation of MeHg and the role of snowmelt runoff and lake stage on persistence of the DBL.

Chapter 3 examines temporal correspondence for trace element concentrations between brine shrimp and water, as well as the relationship between bioaccumulation factors versus trace element concentrations in water and partition efficient. Frequent, co-

located brine shrimp and water column samples were analyzed in order to understand the pathways of trace element transfer from particular locations or water phases to the ecosystem.

## CHAPTER 2

### RESPONSE OF AQUATIC CHEMISTRY AND METHYL MERCURY CONCENTRATION IN GREAT SALT LAKE, UTAH, USA TO ENGINEERED AND HYDROLOGIC FORCINGS

#### 2.1 Abstract

Salinity-driven density-stratified aquatic systems may pose increased contaminant risk due to persistent anoxia at depth, such as in the Great Salt Lake (GSL), Utah, USA, which has elevated methyl mercury (40-90 ng/L) at depth, as well as elevated mercury in waterfowl in adjacent wetlands. Despite its inferred importance, the dynamics of salinity-driven density-stratified systems are not well characterized, particularly in terms of the impact to contaminant cycling. Dramatic decreases of methyl mercury in water and sediment in the GSL were previously reported in response to elimination of limited flow through the earthen railroad causeway separating the North and South Arms of the GSL in late 2013. Reopening of north-south flow in late 2016 offered the opportunity to understand the drivers of density stratification that in turn drive geochemical conditions supporting mercury methylation at depth. The evolution of density stratification following reopening of flow, and its impacts on aquatic chemistry in the midst of hydrologic forcings over larger timescales, demonstrated the relative impacts of engineered versus hydrologic (e.g., snowmelt runoff) forcings on stratification.

Measured aquatic chemistry parameters under destratified versus stratified conditions clarified the role of the deep brine layer versus underlying sediment organic matter in driving methyl mercury accumulation in the GSL.

## 2.2 Introduction

Endorheic or terminal lakes (lacking outflow) occur across the globe, with the largest in area, the Caspian Sea (Russia, Turkmenistan, Iran, Kazakhstan, and Azerbaijan), being also deep and perennially stratified (Boehrer and Schultze, 2008), whereas the 10th largest in area, the Aral Sea (Uzbekistan), no longer supports a fishing industry and now poses dust impact to surrounding populations, in response to inflow diversion and increased lakebed exposure (Wurtsbaugh et al., 2017). Accumulation of toxic trace elements in deeper water and sediment of endorheic lakes is mediated by the overlying water column, which may stratify via seasonal inflow of lower salinity water onto a higher salinity water column, with stratification persistence depending on relative magnitudes of inflow, water column salinity, and wind- and flow-driven mixing (Boehrer and Schultze, 2008; Boehrer et al., 2014; Johnson et al., 2015; Arnon et al., 2016). The internal hydrodynamics of endorheic lakes governs potential accumulation of trace elements in their relatively concentrated waters and underlying sediments (Boehrer and Schultze, 2008; Diaz et al., 2009; Valdes et al., 2015), yet the impact of inflow and other forcings on density-driven stratification, and propagation of these impacts to trace element cycling in endorheic lakes, is poorly understood.

The Great Salt Lake (GSL), located in northwestern Utah, USA (Figure 2.1) is the 5<sup>th</sup> largest endorheic lake in the world, and the largest endorheic lake in the Western

Hemisphere, and is recognized as a site of hemispheric importance by the Western Hemisphere Shorebird Reserve Network, with over 1.4 million shorebirds using the GSL and surrounding wetlands for breeding and staging areas (Aldrich and Paul, 2002), and over seven million water birds utilizing the GSL and its associated wetlands during some portion of their biannual migration (Cline et al., 2011). It is also adjacent to the Salt Lake City - Ogden metropolitan area with a population of approximately 1.5 million. Three duck species at the GSL were found to have breast muscle tissue Hg concentrations exceeding the EPA screening value of 0.3 mg/kg ww (US EPA, 2000; Scholl and Ball, 2005; Scholl and Ball, 2006), resulting in duck consumption advisories being issued for Northern Shovelers, Common Goldeneye, and Cinnamon Teal at the GSL.

During the years 2014 to 2016, a dramatic change occurred in the GSL that was triggered by closure of flow through a railroad causeway, constructed in 1959, that restricted water flow between the North Arm (Gunnison Bay) and the South Arm (Gilbert Bay) (Loving et al., 2000). The North Arm brine is evaporatively concentrated to higher salinity (16 to 29%) than the South Arm brine (6 to 25%) (Stephens et al., 1990) because more than 90% of the freshwater runoff enters the South Arm of the GSL. Prior to 2014, flow of North Arm brine at depth through culverts in the causeway produced a persistent approximately 2-3 thick deep brine layer (DBL) underlying the approximately 6-7 m thick shallow brine layer in the South Arm (Loving et al., 2000; Gwynn, 2002; Naftz et al., 2008; Diaz et al., 2009; Johnson et al., 2015; Valdes et al., 2017). This DBL was not subject to annual turnover despite seasonal wind forcing (Beisner et al., 2009), although periodic destratification events were noted (Naftz et al., 2008; Jones and Wurtsbaugh, 2014). In addition to anoxia, high sulfate-reducing activity and elevated

methyl mercury (MeHg) concentrations, ranging 20 to 30 ng/L (Naftz et al., 2008; Johnson et al., 2015), characterize the DBL, with MeHg being of particular concern since it is the toxic bioaccumulative form of mercury (Mergler et al., 2007).

This study examines the response of the DBL to engineered (causeway flow elimination and reestablishment) and hydrologic (freshwater runoff and lake stage) forcings, and their impact on MeHg concentrations and potential production. Destratification of the GSL within 6 months of culvert (width = 4.6 m, depth = approximately 6 m) closure in December 2013, to form an oxic vertically homogeneous water column free of dissolved sulfide and with dramatically reduced MeHg concentration in deep water (86%) and underlying surficial sediment (77%), was previously reported (Valdes et al., 2017). Subsequent high temporal frequency data collected following engineered breach (width = 45.7 m, depth = 4.9 m) of the causeway in December 2016 offer a grand opportunity to examine evolution of the aquatic and trace element chemistry in the GSL in response to reestablishment of flow as well as ambient hydrologic variations. Our findings provide understanding of the impacts of potential engineered impoundments in endorheic lakes within their hydrologic context, and extend observations of density-driven stratification to impacts on accumulation of MeHg and other trace elements.

### 2.3 Methods

#### 2.3.1 Locations

During July 2016 to May 2018, water and surficial sediment from six sites (CB2, 2565, N1018, 3510, GB14, and 4069) in the South Arm (Gilbert Bay) of the GSL were

analyzed for concentrations of THg, MeHg, trace elements, DOC, major ions, sulfide, and density (Figure 2.1). Both unfiltered and filtered (0.45 µm PES membrane) shallow waters (0.2 m below water surface) and deep waters (0.5 m above bottom) were collected. The target sediment was the unconsolidated, surficial sediment slurry (SSL). THg, MeHg, and trace element samples were collected in triplicate; other samples were collected in duplicate. The data from these samples were compared to results from the same matrices collected previously from 2006 to 2015 (Diaz et al., 2009; Johnson et al., 2015; Valdes et al., 2017). In addition to the above six sites, surficial sediment was collected nearby site 3510 from sites B1 and B2 in 2012, and from sites C1 and C2 nearby site 2565 in 2012 (Figure 2.1). Water density, temperature, and lake elevation were obtained from USGS data ([https://waterdata.usgs.gov/nwis/inventory?agency\\_code=USGS&site\\_no=10010026, 20181222](https://waterdata.usgs.gov/nwis/inventory?agency_code=USGS&site_no=10010026, 20181222)).

### 2.3.2 Sampling and Analyses

#### 2.3.2.1 THg and MeHg

Clean hands–dirty hands protocol was followed during sample collection and analysis (US EPA, 1996). Unfiltered water samples were collected by peristaltic pump using acid-washed PTFE tubing into precleaned FLDPE and PTFE bottles that were pre-filled with trace metal grade (TMG) sulfuric acid to preserve samples with 0.5% acid. Filtered water samples were passed through 0.45 µm pore size, preacid-rinsed capsule filters (Geotech Environmental) in the field. All water samples were stored in the dark on ice in the field, refrigerated in the lab, and analyzed within 3 weeks of collection.

SSL samples were collected in acid-washed FLDPE bottles and filled to overflowing to minimize exposure to air by peristaltic pump with the end of the Teflon tubing weighted with a plastic-coated weight. Sediment samples were stored on ice in the field, transferred to a freezer in the laboratory, and analyzed within 6 months of collection.

Water samples for THg analysis were oxidized by amendment to 2-5% BrCl back in the lab. This higher BrCl concentration relative to established protocols was necessary to fully oxidize the high levels of sulfide and dissolved organic matter in some water samples (as described below). THg concentrations in water were determined via reduction with SnCl<sub>2</sub>, purge and trap onto gold traps, thermal desorption, with quantification by cold vapor atomic fluorescence spectroscopy (CVAFS) using a MERX-T automated system (Brooks Rand) using established techniques (US EPA, 2002). The USGS certified reference material (CRM) Hg64 for THg in water was included in multiple analyzes, with recoveries averaging 85%. MeHg concentrations in water were measured after distillation with ammonium pyrrolidine dithiocarbamate (APDC), followed by aqueous-phase ethylation, purge and trap onto tenax traps, thermal desorption, pyrolytic decomposition, and CVAFS detection using a MERX-M automated system (Brooks Rand) using established techniques (US EPA, 2001).

SSL samples for THg analysis were extracted from sediment using a 7:3 mixture of HNO<sub>3</sub>:H<sub>2</sub>SO<sub>4</sub> (trace metal grade) at 80 °C for 6 h, followed by amendment to 5% BrCl (US EPA, 2002). MeHg was leached from sediment with a mixture of potassium bromide, sulfuric acid, and copper sulfate, extracted into methylene chloride, back-extracted into water, followed by aqueous-phase ethylation, purge and trap, thermal

desorption, pyrolytic decomposition, and CVAFS detection according to established techniques (US EPA, 2001; Bloom et al., 1997). Subsamples were oven-dried at 105 °C for 12 h and reweighed to determine water content and allow conversion between wet weight (ww) and dry weight (dw) concentrations (without salt correction). CRMs for THg (MESS-3, Research Council Canada) and MeHg (CC-580) in sediment were also analyzed.

#### 2.3.2.2 Mercury Methylation/Demethylation Incubation Experiments

Unfiltered deep water and sediment samples used in mercury methylation/demethylation lab experiments were collected as described above, except they were not preserved with acid. These samples were filled to overflowing to minimize headspace and to avoid exposing anoxic samples to oxygen.

Mercury methylation and demethylation rates were determined in select sediment and deep water samples spiked with  $^{204}\text{iHg}$  and  $\text{Me}^{201}\text{Hg}$ , respectively. These samples were prepared under argon in a glove box (Vacuum Glovebox VGB, MTI Corporation) at room temperature within 12 h of sample collection. Isotope tracer concentrations were targeted to match ambient THg and MeHg concentrations (total of all isotopes). However, not all ambient THg and MeHg concentrations were known a priori, in which case estimates were made based on previously existing data.  $^{204}\text{iHg}$  and  $\text{Me}^{201}\text{Hg}$  amendments were made to each sample aliquot (200 g water, 50 g sediment slurry) and homogenized by stirring.

Following isotope addition, samples were subdivided to allow multiple incubation times in parallel subsamples. Subsamples were placed into crimp-top serum bottles with

chlorobutyl-isoprene septa (50 mL bottles for water, 10 mL bottles for sediment).

Subsamples were replicated to allow analysis of pre- and postamended samples (duplicates for each pre- and postamended sample), and to allow correction for extraction inefficiencies via isotope dilution (described below). Subsample incubations were performed at room temperature (19–21°C) in the dark on a shaker table (130 rpm). Incubations were ended after 2 h via the addition of TMG HCl to 1% vol/vol and refrigeration for water, or via flash freezing in an ethanol bath with dry ice for sediment.

An isotope dilution (ID) spike of  $\text{Me}^{200}\text{Hg}$  was added to samples via glass syringe prior to MeHg distillation for water or prior to MeHg extraction for sediment. The ID spike concentrations were matched to ambient MeHg concentrations. Following ID spike addition, the samples were allowed to equilibrate for 30 minutes before distillation or extraction. Hg methylation/demethylation experiment samples were analyzed within 1 month for water and 3 months for sediment slurry.

#### 2.3.2.3 DOC, Major Ions, Sulfide, and Ancillary Field Parameters

Filtered water samples were collected as described above into precleaned LDPE bottles. Bottles were filled to overflowing to minimize the headspace, then stored as above, and analyzed within 3 weeks of collection. DOC samples were diluted 10-fold with high-purity water to reduce the salt interference and then analyzed by the combustion catalytic oxidation method using a total organic carbon analyzer (Shimadzu TOC-L). Major ions samples were diluted 500-fold to be in the linear working range then measured via ion chromatograph (Metrohm 883 Basic IC plus). Water density was determined gravimetrically in unfiltered samples. Sulfide was measured in 0.45  $\mu\text{m}$

filtered water in the field immediately after collection using a CHEMetrics kit (V-2000 Multi-analyte LED Photometer and Vacu-vials®).

Water column depth profiles of dissolved oxygen (DO), specific conductance (SpC), and temperature were measured in the field at depths starting from approximately 0.2 m below the surface to the bottom using a field probe (In Situ Inc. Troll 9500 multi-parameter water quality sonde). DO data reported prior to July 2016 by USGS ([https://waterdata.usgs.gov/nwis/inventory?agency\\_code=USGS&site\\_no=10010026, 20181222](https://waterdata.usgs.gov/nwis/inventory?agency_code=USGS&site_no=10010026, 20181222)) were not salinity corrected, whereas we salinity corrected these DO values using a relationship between corrected and uncorrected values (post 2016) incorporating specific conductance and temperature.

#### 2.3.2.4 Methylation Kinetic Analysis

Isotope dilution (ID) was used to correct for MeHg extraction inefficiencies in determining isotope concentrations, based on recovery of the ID isotope (Me<sup>200</sup>Hg) as follows (Hintelmann and Evans, 1997).

$$C_{204}^{preID} = \frac{m_{204}^{Me200ID} \left( R_{\frac{200}{204}}^{Me200ID} - R_{\frac{200}{204}}^{postID} \right)}{\text{sample mass} \left( R_{\frac{200}{204}}^{postID} - R_{\frac{200}{204}}^{preID} \right)}$$

where,  $C_{204}^{preID}$  is the ID-corrected concentration of Me<sup>204</sup>Hg,  $m_{204}^{Me200ID}$  is the mass of Me<sup>204</sup>Hg in the enriched Me<sup>200</sup>Hg ID spike,  $R_{200/204}^{Me200ID}$  is the ratio of Me<sup>200</sup>Hg to Me<sup>204</sup>Hg in the ID spike,  $R_{200/204}^{postID}$  is the ratio of Me<sup>200</sup>Hg to Me<sup>204</sup>Hg in the sample post-ID spike addition,  $R_{200/204}^{preID}$  is the ratio of Me<sup>200</sup>Hg to Me<sup>204</sup>Hg in the sample pre-ID spike addition, and *sample mass* corresponds to the mass of sample to which the ID spike was added.

The percentage of the Me<sup>204</sup>Hg increase during the 2 h incubation (% Me<sup>204</sup>Hg increase) was calculated as:

$$\% \text{Me}^{204}\text{Hg Increase} = \frac{C_{\text{Me}204\text{Hg}}^{2hID} - C_{\text{Me}204\text{Hg}}^{\text{initial}} - C_{\text{Me}204\text{Hg}}^{\text{spiked}}}{C_{\text{Me}204\text{Hg}}^{\text{initial}} + C_{\text{Me}204\text{Hg}}^{\text{spiked}}} \times 100\%$$

where,  $C_{\text{Me}204\text{Hg}}^{2hID}$  is the ID-corrected concentration of Me<sup>204</sup>Hg after the 2 h incubation,  $C_{\text{Me}204\text{Hg}}^{\text{initial}}$  is Me<sup>204</sup>Hg concentration of sample at the start of the incubation, and  $C_{\text{Me}204\text{Hg}}^{\text{spiked}}$  is the concentration of spike Me<sup>204</sup>Hg added.

The percentage of the Me<sup>201</sup>Hg decrease during the 2 h incubation (% Me<sup>201</sup>Hg decrease) was calculated as:

$$\% \text{Me}^{201}\text{Hg Decrease} = \frac{C_{\text{Me}201\text{Hg}}^{\text{initial}} + C_{\text{Me}201\text{Hg}}^{\text{spiked}} - C_{\text{Me}204\text{Hg}}^{2hID}}{C_{\text{Me}201\text{Hg}}^{\text{initial}} + C_{\text{Me}201\text{Hg}}^{\text{spiked}}} \times 100\%$$

where,  $C_{\text{Me}201\text{Hg}}^{2hID}$  is the ID-corrected concentration of Me<sup>201</sup>Hg after the 2 h incubation,  $C_{\text{Me}201\text{Hg}}^{\text{initial}}$  is Me<sup>201</sup>Hg concentration of sample at the start of the incubation, and  $C_{\text{Me}201\text{Hg}}^{\text{spiked}}$  is the concentration of spike Me<sup>201</sup>Hg added.

## 2.4 Results

### 2.4.1 Engineered Destratification and Restratification

Evolution of the GSL water column in response to causeway reopening is described below in the longer term context beginning prior to culvert closure and continuing to the present. Closure of the last culvert in December 2013 (Figure 2.2 left-most grey vertical bar) destratified the GSL approximately 6 months after closure, as shown by convergence of the contrasting densities in deep (0.5 m above bottom) (Figure 2.2 blue squares) and shallow (0.2 m below surface) (Figure 2.2 red triangles) waters. Concomitant with this density destratification, DO converged, increasing in deep (Figure

2.2 blue dashed lines) and decreasing in shallow (Figure 2.2 red dotted lines) waters.

Prior to culvert closure, the predominant anoxic, sulfate-reducing conditions in the DBL generated elevated concentrations of sulfide (12-18 mg/L, Figure 2.3), DOC (60-80 mg/L, Appendix A), MeHg (15-35 ng/L, Figure 2.3), and THg (40-90 ng/L, Figure 2.4), with the shallow brine having significantly lower concentrations of these analytes, consistent with oxic conditions (Johnson et al., 2015; Valdes et al., 2017).

After culvert closure, dramatic reductions (50-90%) in the concentrations of sulfide, MeHg, and THg in deep waters occurred, converging with shallow water concentrations, in response to destratification of the South Arm (Figures 2.3, 2.4), as previously reported (Valdes et al., 2017). Notably, even under destratified conditions from summer 2014 to summer 2017, deep waters of the South Arm experienced seasonal anoxia in response to snowmelt runoff (Figure 2.2), under which conditions MeHg concentrations were temporarily increased at depth (3-8 ng/L) sometimes without detectable increased sulfide (Figure 2.3, Appendix A). The most dramatic of these events (spring 2017) followed a relatively large snowmelt runoff (Figure 2.3, Appendix A), as explored below. The snowmelt runoff drove temporary freshwater/brine stratification distinct from the brine/brine stratification driven by flow from North Arm.

The causeway was breached in December 2016 (Figure 2.2 intermediate grey vertical bar), but water flow was initially exclusively from the South to North Arm due to the head differential that accumulated during elimination of flow between the two arms. North-to-south flow was first detected (by monthly monitoring) in early July, 2017 (Figure 2.2 right-most grey vertical bar) and initiated restratification with divergence of water densities (deep increasing, shallow relatively constant) and DO (deep decreased,

shallow increased) (Figure 2.2). North-to-south flow was averaged approximately 14 m<sup>3</sup>/s, higher in summer (14 to 28 m<sup>3</sup>/s) and lower in winter (4.5-11 m<sup>3</sup>/s) ([https://waterdata.usgs.gov/nwis/inventory?agency\\_code=USGS&site\\_no=10010026, 20181222](https://waterdata.usgs.gov/nwis/inventory?agency_code=USGS&site_no=10010026, 20181222)).

Consistent with north-to-south flow, restratification started in the north and progressed southward with time (Figure 2.5), with restratification initiated in July 2017 at sites CB2 and 2565, in August 2017 at site N1018, later in Fall 2017 at site 3510, and in Spring 2018 at site GB14 (Figure 2.5), with the shallower water column at site 4069 (4-5 m) never becoming stratified (Figure 2.5, Appendix A). As of May 2018, the thickness of the reemerging DBL was greatest at the north and decreased moving south (Figure 2.5), with an approximate thickness of 2.9 m at CB2, and 0.9 m at GB14, the southernmost site where stratification occurred. Similarly, the contrast in the density of shallow and deep waters was greatest at the northernmost site CB2 (0.07 g/cm<sup>3</sup>) and decreased moving south to a difference of only 0.03 g/cm<sup>3</sup> at the southerly site GB14 (Appendix A). The slightly lower density of DBL at site 3510 (~ 1.13 g/cm<sup>3</sup>) relative to site 2565 (~ 1.15 g/cm<sup>3</sup>) under brine/brine stratified conditions (Figure 2.2) indicates modest mixing during north-to-south transport between the sites. Major ion (chloride, sodium, potassium, sulfate) concentrations in surface and deep waters during this time (Appendix A) exhibited temporal and spatial trends similar to density (Appendix A) and specific conductance (Figure 2.5). Restratiification was periodically interrupted at site N1018 in September, 2017 (Figure 2.5, Appendix A), indicating the pooling deep brine was subject to mixing by wind or other processes at the relatively low lake elevations during this period (Figure 2.2).

Restratification from North Arm flow yielded changes in deep waters including decreased DO, and increased sulfide, DOC, THg, and MeHg (Figures 2.2, 2.3, 2.4, Appendix A). At sites 2565 and 3510, deep water concentrations of DOC increased by 40-70% to 80-100 mg/L (Appendix A), sulfide increased to 3-15 mg/L (Figure 2.3), MeHg increased to 14-23 ng/L (Figure 2.3), and THg increased to 17-55 ng/L (Figure 2.4). During this same time period, concentrations of these same parameters remained relatively unchanged in surface waters (Figures 2.3, 2.4, Appendix A). The temporary interruption of DBL development (at N1018 in September, 2017) coincided with decreased concentrations of MeHg and sulfide in deep waters (Appendix A).

Ongoing reestablishment of the DBL resulted in concentrations of a number of analytes increasing towards levels observed prior to 2014 prior to culvert closure (Figures 2.2, 2.3, 2.4, Appendix A). MeHg concentrations in surficial sediment have not increased significantly in response to restratification to date (Figure 2.6). Average MeHg concentrations in sediment at site 3510 in November 2017 ( $0.31 \pm 0.28$  ng/g) following initiation of DBL redevelopment were still indistinguishable to those measured in 2015-2016 after destratification ( $0.23 \pm 0.56$  ng/g) (Valdes et al., 2017), and remained well below those observed prior to culvert closure in late 2013 ( $1.53 \pm 0.1$  ng/g) when the DBL was robust (Johnson et al., 2015). This was also true for MeHg in sediment at the five other sites (Appendix A). THg concentrations in surficial sediment were variable (within a factor of two), with no statistically significant ( $p > 0.05$ ) changes occurring during the entire process of South Arm destratification and restratification from prior to 2014 until early 2018 (Figure 2.6 and Appendix A).

Incubation experiments examining %  $\text{Me}^{204}\text{Hg}$  increase and %  $\text{Me}^{201}\text{Hg}$  decrease

in spiked deep water and surficial sediments showed no statistically significant difference ( $p > 0.05$ ) under stratified versus destratified conditions (Appendix A), although the two highly elevated values of % Me<sup>204</sup>Hg increase were associated with stratified conditions (Appendix A site 2565). Negative values % Me<sup>204</sup>Hg increase and % Me<sup>201</sup>Hg decrease on the order of 100% (factor of two) were common (Appendix A). If the negative values had corroborated each other, they might indicate strong methylation and demethylation of ambient Me<sup>204</sup>Hg and ambient Me<sup>201</sup>Hg, respectively. The lack of corroborating negative values (Appendix A) indicates that they represent error in the analyses, such that only those % methylation or % demethylation values exceeding 100% were considered significant.

## 2.5 Discussion

### 2.5.1 Influences of Hydrologic Context

The above-described engineered transition lies within a hydrologic context wherein interannual variation in snowmelt runoff yields variation in lake surface elevation and water column depth (Figure 2.2). The 3 years prior to 2014 and culvert closure coincided largely with higher lake elevation; however, fall 2010 to winter 2011 was a period of relatively low lake elevation (< approximately 1279 m), during which time (and before) the DBL was absent in the south basin of the South Arm of the GSL (Figure 2.2 bottom panel) and was briefly displaced in the north basin of the South Arm (Figure 2.2 top panel), likely by seiche (Beisner et al., 2009).

Density of shallow water varies inversely with lake elevation, as does deep water density under destratified conditions (Figure 2.2), such as prior to summer 2011 at

southern site 3510, and at both northern and southern South Arm sites (2565 and 3510) following culvert closure in December 2013 through first-detected north-to-south flow in summer 2017. Under density-stratified conditions, DBL density did not correspond inversely with lake elevation (Figure 2.2). Initiation of density stratification in both basins of the South Arm (Figure 2.2), and decoupling of DBL density from lake elevation, occurred in Spring 2011 during runoff from an extremely large snowpack, which resulted in a nearly 1.5 m increase in lake elevation (Cordova and Angeroth, 2012).

The largest temporary anoxic event at depth under destratified conditions, when lake stage was relatively low (< approximately 1279 m), occurred in response to the relatively large February 2017 snowmelt runoff event (Figure 2.2). The southward propagation of snowmelt runoff from the Bear River (largest flow into GSL) is shown by specific conductance (Figure 2.5). Low conductivity appeared in shallow waters first in the northern sites of the South Arm (CB2, 2565, and N1018) and then later into the southern sites (3510, GB14, and 4069) (Figure 2.5). A 30-40% decrease in the specific conductance initially occurred at the surface, propagating southward and deeper with time (Figure 2.5). Along with the previously described temporary increases in deep water sulfide (2-6 mg/L) and MeHg (8-13 ng/L) (Figure 2.3), increases in THg (20-40 ng/L, Figure 2.4) were observed, again at depth only (Figures 2.3, 2.4, Appendix A). These increases were not associated with sediment resuspension, as both THg and MeHg remaining predominantly in the dissolved phase in deep water during these events (Appendix A), although some instances of particle-bound THg suspension were observed (Appendix A). The deep water particulate fractions of MeHg and THg were generally

high when MeHg concentrations in deep waters were low (Appendix A).

### 2.5.2 Combined Influences of Engineered and Hydrologic Perturbations

Engineered closing and reopening of flow through the railroad causeway produced dramatic changes in GSL as described above. A 6-month lag was observed between causeway closure and destratification, as well as between causeway opening and restratification (Figure 2.2). Based on an average north-to-south flow of  $14 \text{ m}^3/\text{s}$  ([https://waterdata.usgs.gov/nwis/inventory?agency\\_code=USGS&site\\_no=10010026, 20181222](https://waterdata.usgs.gov/nwis/inventory?agency_code=USGS&site_no=10010026, 20181222)), the time to reestablish the estimated preclosure DBL volume of  $1\text{ km}^3$  (Valdes et al., 2017) is 26 months, suggesting that the restratification reported here reflects approximately one third of the time needed to refill the preclosure DBL volume. The processes governing the 6-month lag time associated with: a) destratification; b) initiation of north-to-south flow upon reopening; and c) restratification, are outside the scope of this work, but certainly involve the time needed for equilibration of hydraulic heads via shallow south-to-north, and deep north-to-south, brine flows through the causeway, as well as seepage through the causeway material. Notably, change in the direction of net flux through the causeway culverts follows by approximately 6 months the maximum elevation difference between the North and South Arms (Jewell, 2018).

A novel insight is that under destratified conditions and relatively low lake stage (< 1279 m), relatively large snowmelt runoff events yielded temporary anoxia at depth, along with temporary increases in THg and MeHg concentrations in deep waters (Figures 2.2 and 2.3). This is shown, for example, by a relatively large snowmelt runoff event and

1 m lake stage increase in 2017, after which DO decreased (Figure 2.2) and sulfide and MeHg increased (Figure 2.3) at northern and southern sites (2565 and 3510). The exceptionally large snowmelt in spring of 2011 was also followed by DO depression at depth at site 3510 where the water column was previously destratified (Figure 2.2).

### 2.5.3 Role of Underlying Sediment

Our observation that deep water DO increased in the Fall of 2010, 2014, 2015, and 2016, during which years the annual minimum in lake elevation was less than 4194 feet (Figure 2.2), corroborates the expectation that GSL deep water is vulnerable to wind-driven mixing under low stage conditions (Naftz et al., 2008; Jones and Wurtsbaugh, 2014), as controlled by physical factors such as lake fetch, internal wave period, and the velocity and duration of wind events (Rueda and Schladow, 2009).

Our observations (Figure 2.2) demonstrate annual minima in South Arm surface water DO concentrations during summer and fall, as previously reported (Belovsky et al., 2011) and attributed to increased organic carbon abundance and decreased O<sub>2</sub> production associated with decreased phytoplankton abundance due to predation by brine shrimp (Belovsky et al., 2011). Whereas this highlights the role of organic carbon cycling in the water column, the water column DO data also suggest a strong role of organic carbon in underlying surficial sediment. DO in the water column responded consistently to the presence versus absence of brine/brine stratification, wherein DO levels contrasted dramatically between deep (largely anoxic) and shallow (oxic) waters under brine/brine stratified conditions (Figure 2.2), but where DO levels converged among shallow and deep waters during destratification, with relatively depressed DO in the shallow water

column (Figure 2.2). General depression of surface water DO concentrations under conditions absent the DBL strongly implicates oxygen demand by organic matter in underlying surficial sediment under destratified (mixed) conditions. Anecdotal reports from samplers indicated that organic matter thickness was greatly decreased following the extended destratified conditions of summer 2014 to summer 2017.

#### 2.5.4 Role of DBL

Elevated sulfide, as well as elevated sulfate and DOC, at depth progressed from north-to-south with reestablishment of the DBL (Appendix A), demonstrating that re-establishment of the DBL increased sulfate reduction. MeHg comprises approximately 50% and approximately 5% of THg in the DBL under stratified and destratified conditions, respectively (Appendix A). However, dramatically decreased MeHg and THg concentrations in deep water in response to destratification (approximately ten-fold and five-fold, respectively) (Appendix A) suggest that the DBL promotes accumulation of both THg and MeHg in the deep water column. Based on the above observations, the presence of the DBL apparently limits upward propagation of oxygen demand from underlying sediment organic carbon into surface waters, thereby allowing in deep waters the accumulation of sediment organic matter, promotion of sulfate reduction, and production and accumulation of MeHg.

That the north-to-south conveyance of the DBL renders it independent of shallow water is evidenced by its de-coupling from lake elevation (inversely phased for shallow water) under destratified conditions (summer 2014 to summer 2017) (Figure 2.2). This “conveyor belt” nature of the DBL is consistent with the high velocities (up to 55 cm/s)

measured for DBL flow across the topographic saddle separating the north and south basins of the South Arm (Naftz et al., 2014), as well as the observed periodic elimination and rapid reestablishment of the DBL during restratification (Figure 2.2). Conveyance of the DBL likely promotes its independence from shallow water and likely enhances its serving as a sort of cap (Johnson et al., 2015; Valdes et al., 2017) under which MeHg and organic matter accumulate in the DBL and SSL. Mixing of DBL into the overall water column at GSL's southern terminus (e.g., between sites GB14 and 4069) must occur, although little is known about the dynamics of entrainment of the southward moving DBL.

The above observations indicate that the chemical characteristics of the GSL's water column are governed by several forcings: one being denser brine inflow from the North Arm that can produce brine/brine stratification, a second being oxygen demand from accumulated organic matter in the underlying surficial sediment, and a third being snowmelt runoff that can produce freshwater/brine stratification.

### 2.5.5 Sources and Pathways

Because of their strong sulfate-reducing activity and elevated MeHg concentrations, the DBL and underlying surficial sediment are implicated as a reservoir from which MeHg propagates into biota in the GSL and surrounding wetlands (Naftz et al., 2008; Vest et al., 2009; Wurtsbaugh et al., 2011; Saxton et al., 2013; Johnson et al., 2015). However, the GSL ecosystem beyond bacteria (e.g., phytoplankton, brine shrimp, brine flies, insects, and birds) resides in the shallow brine and surrounding wetlands. The mechanism by which MeHg in the DBL propagates to the overlying and adjacent

ecosystem is undetermined, although anecdotal evidence for potential migration of brine shrimp to the DBL interface has been reported (Jones and Wurtsbaugh, 2014). Temporal correspondence of THg concentrations in brine shrimp and shallow filtered brine was observed under destratified conditions (Yang et al., 2019).

That % Me<sup>204</sup>Hg increase did not contrast under stratified versus destratified conditions in either the deep water or surficial sediment (Appendix A) suggests that the role of the DBL was to promote accumulation, rather than promote increased MeHg production. Relatively low % Me<sup>204</sup>Hg increase and % Me<sup>201</sup>Hg decrease in deep water and surficial sediment (Appendix A) indicated that MeHg concentrations were governed not only by in situ methylation/demethylation, but as well by other geochemical and transport processes. Notably, under destratified conditions, temporary increases in MeHg concentrations (i.e., July 2016) were largely coincident in deep and shallow waters, with typically higher values in deep (3-8 ng/L) relative to shallow (1-3 ng/L) waters (Figure 2.3). This suggests transfer of MeHg from deep to shallow water, possibly by shear-driven entrainment of DBL into the overall water column, and further suggesting a pathway for Hg transfer from deep water to biota.

The inadvertent experiment provided by culvert closure and breach opening provided the opportunity to evaluate the impact of management of north-south flow through the railroad causeway that separates the North and South Arms of GSL. Our observations indicate that elimination of flow between the two arms dramatically reduces MeHg accumulation in the bottom waters of GSL, and reopening of flow returns the system toward MeHg accumulation at depth.

Our results indicate that the MeHg reservoir at depth in GSL may be eliminated

by either complete elimination of flow or by complete mixing between the two arms. This finding is relevant to potential engineered impoundments in other endorheic lakes, for which GSL demonstrates that partitioning a endorheic lake into areas with contrasting inflows can produce salinity-driven density stratification if incomplete mixing between partitions occurs. Density-driven stratification can exacerbate contamination issues via the formation of a persistent anoxic layer at depth within which organic material and toxic trace elements can accumulate.

## 2.6 Acknowledgement

This research was supported by funding from the Utah Divisions of Forestry, Fire, and State Lands (FFSL) of the Utah Department of Natural Resource (180608) program from Utah Division of Water Quality, and the National Science Foundation Low Temperature Geochemistry and Geobiology Program (EAR 1637196). Any opinions, findings, and conclusions or recommendations expressed in this material are those of the authors and do not necessarily reflect the views of the FFSL, Utah Division of Water Quality, and National Science Foundation.

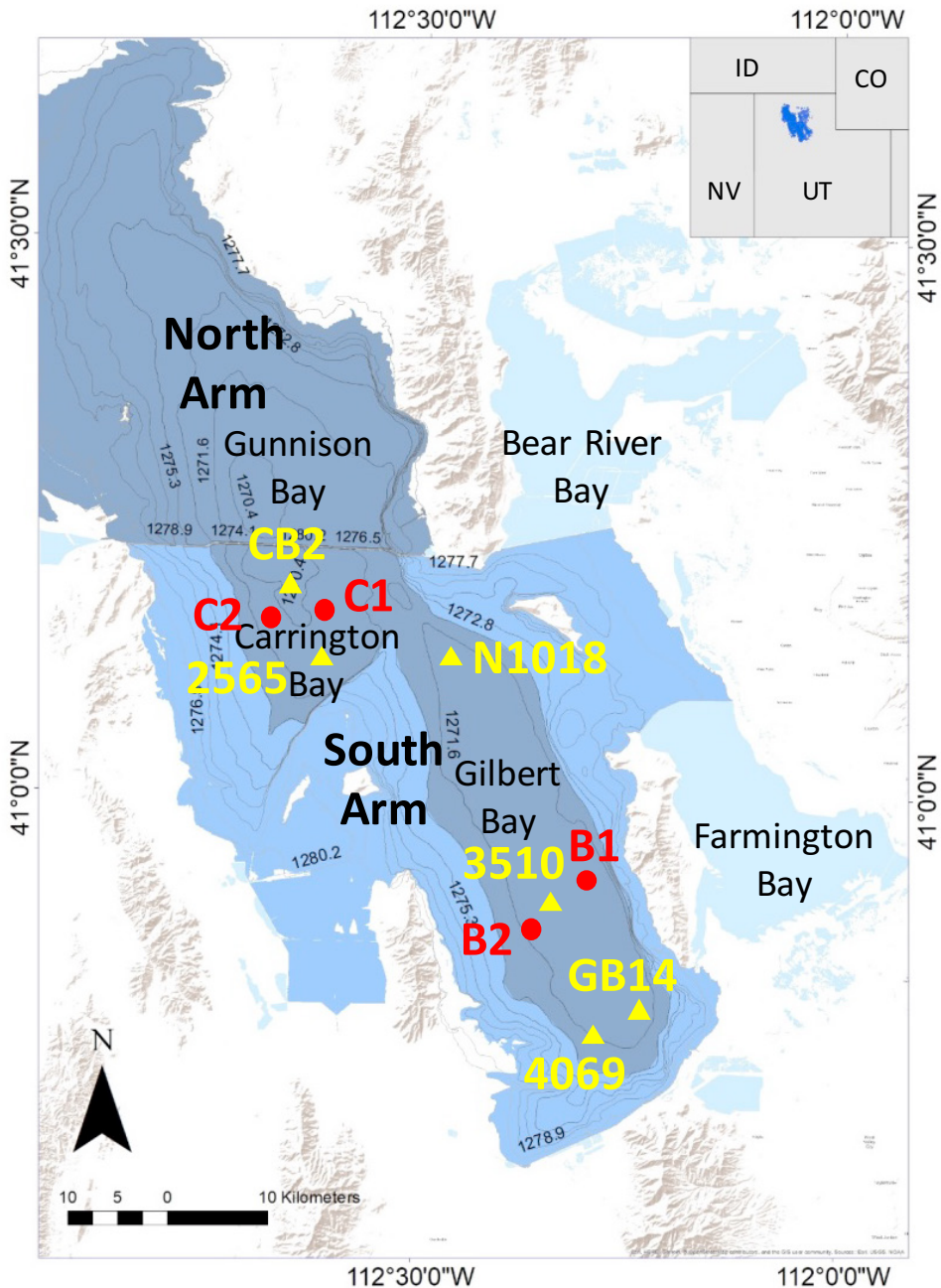


**Figure 2.1.** The Great Salt Lake with sample sites. Triangles represent the sample locations collected from 2006 to 2018. Circles represent additional surface sediment layer (SSL) and methylation sample sites in 2012. Contour intervals represent elevation above MSE in meters. Shading represents typical water salinities (% total dissolved solids) of deep waters during 2007-2012, with gray corresponding to approximately 28%, dark blue corresponding to approximately 15%, and the light blue representing salinities less than 5%. Thus, the darker shading in the South Arm indicates the approximate extent of the deep brine layer until 2012.

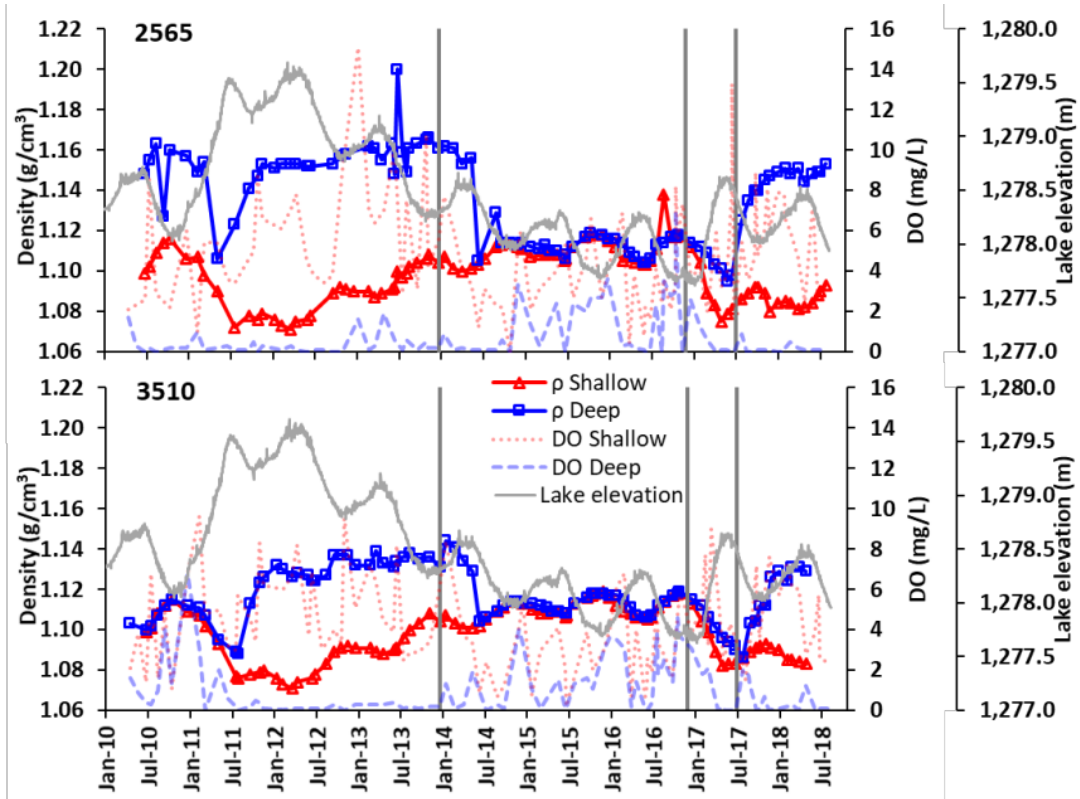


**Figure 2.2.** Density of shallow (red solid lines with triangles) and deep (blue solid lines with squares) brines. Dissolved oxygen (DO) in shallow (0.2 m below surface) (red dotted lines) and deep (0.5 m above bottom) (blue dashed lines). Density and DO values were measured at site 2565 (top panel) and site 3510 (bottom panel). Lake elevation (grey lines) was measured at Saltair Boat Harbor. Grey vertical bars from left to right represent the timing of the closure of the second railroad causeway culvert (December 2013), opening of the new bridge breach (December 2016), and first-detected (monthly monitoring) north-to-south flow through new breach (July 2017).

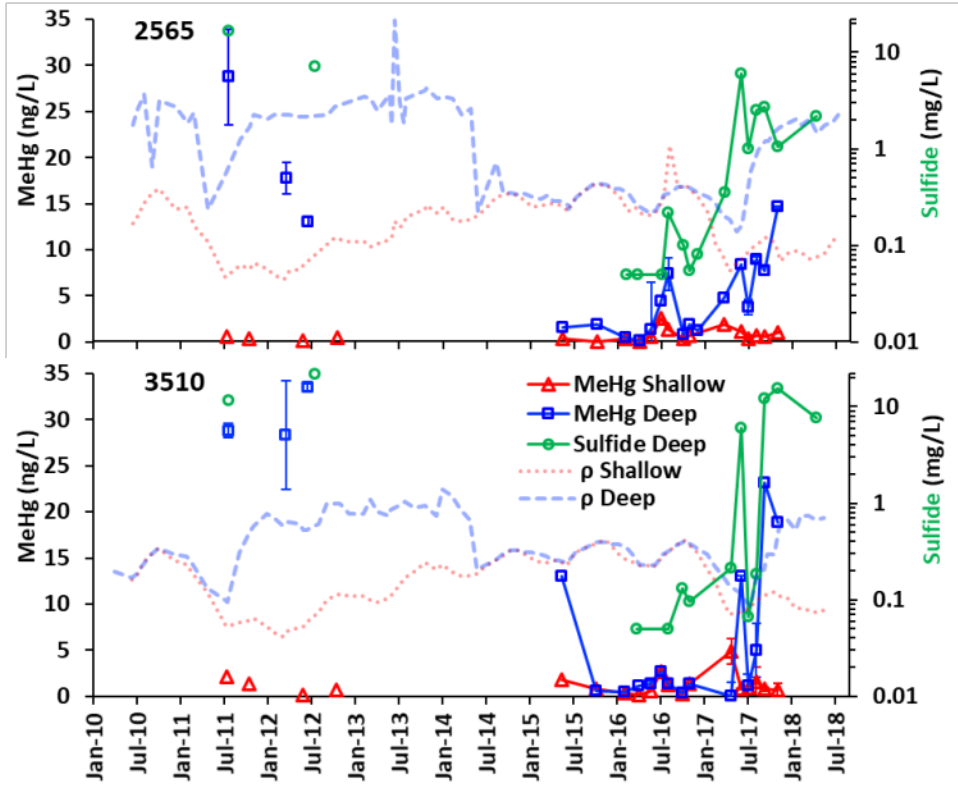


**Figure 2.3.** Unfiltered methyl mercury (MeHg) concentration (mean  $\pm$  standard deviation) and density of shallow and deep waters of the GSL (red triangles and blue squares, respectively) from 2010 to 2018, along with dissolved sulfide in deep waters (green circles) at sites 2565 and 3510 (top and bottom panel, respectively). Red dotted and blue dashed lines represent shallow and deep water density, respectively, and density scale omitted for simplicity; see Figure 2.2.

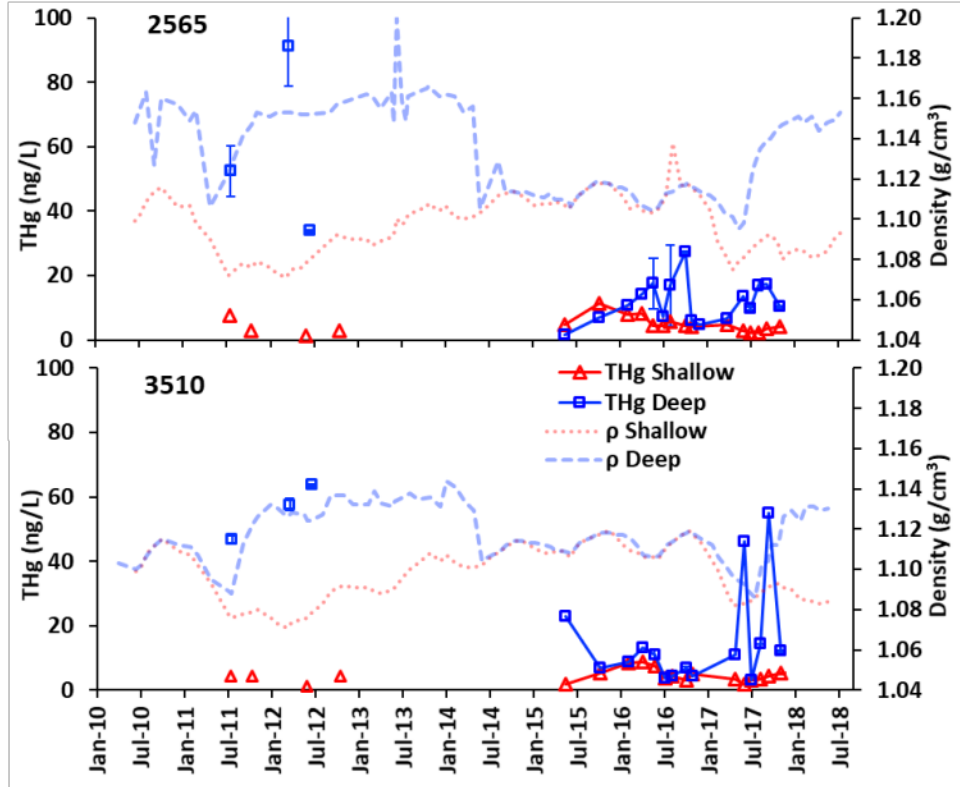


**Figure 2.4.** Unfiltered total mercury (THg) concentrations in shallow and deep waters (red triangles and blue squares, respectively) and density of shallow and deep waters (dotted and dashes lines, respectively) at sites 2565 and 3510 (top and bottom panel, respectively). Red dotted and blue dashed lines represent shallow and deep water density, respectively, and density scale omitted for simplicity; see Figure 2.2.

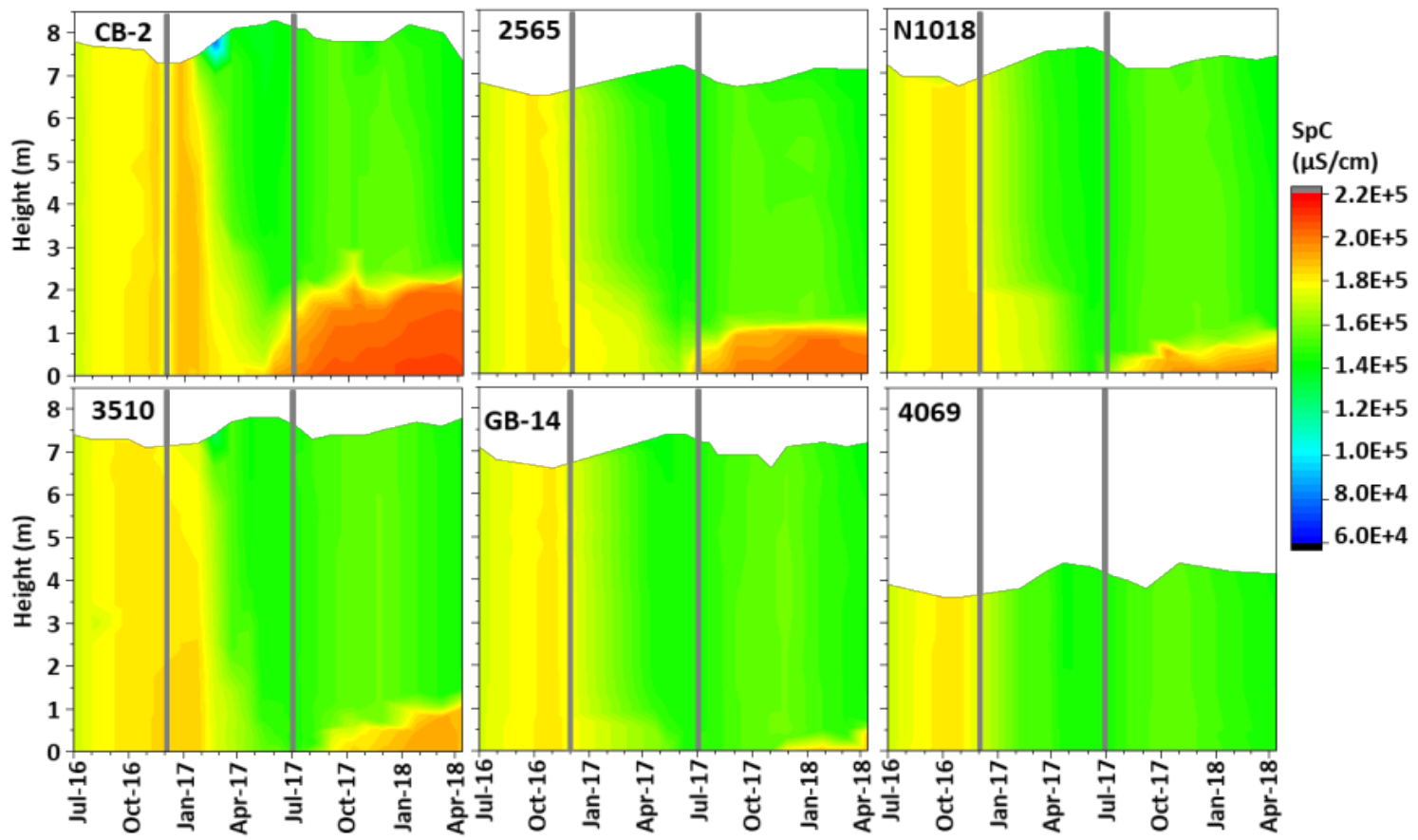


**Figure 2.5.** Specific conductance (SpC) versus height above bottom at the six monitored sites spanning the period of restratification (June 2016 to May 2017). Grey vertical bars in each panel represent opening of bridge breach December 2016 (left bar), and first-detection (monthly monitoring) of north-to-south flow through the new breach July 2017 (right bar).

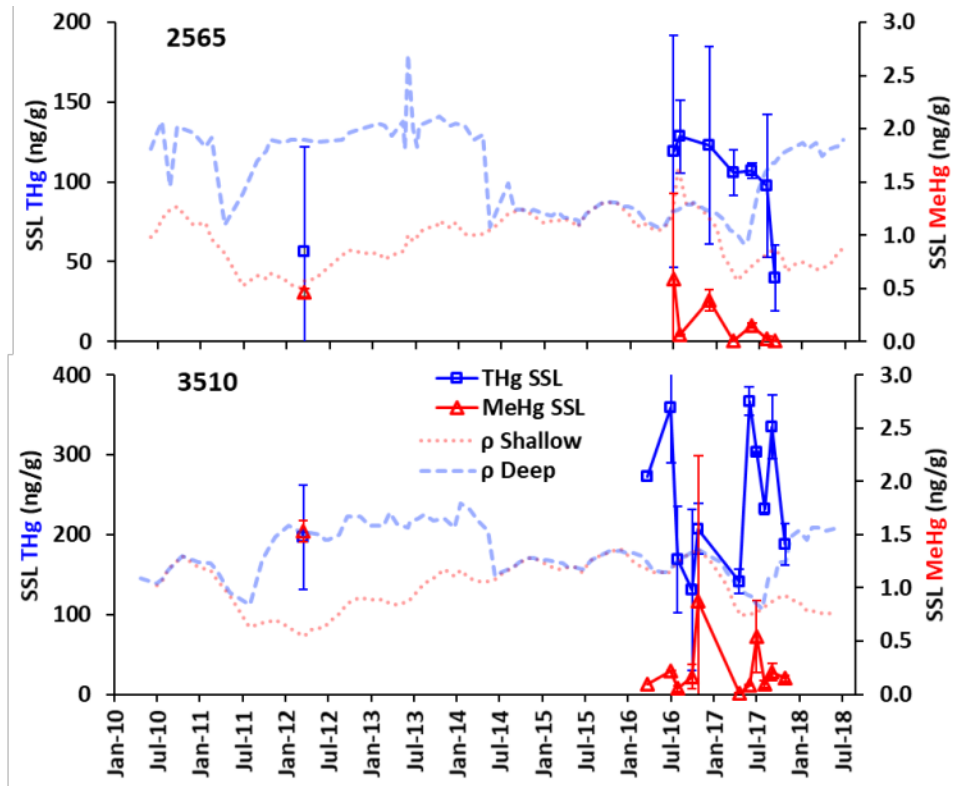


**Figure 2.6.** Surficial sediment (SSL) THg and MeHg concentrations (mean  $\pm$  standard deviation, red triangles and blue square, respectively) and surface water and deep water densities (dotted and dashed lines, respectively) at sites 2565 and 3510 (top and bottom panel, respectively) from 2010 to 2018. Water density scale omitted for simplicity; see Figure 2.2.

## CHAPTER 3

### TEMPORAL CORRESPONDENCE AND PARTITIONING OF SELENIUM AND MERCURY AMONG BRINE SHRIMP AND WATER IN GREAT SALT LAKE, UTAH, USA

#### 3.1 Abstract

Salinity-driven density-stratified aquatic systems may pose increased contaminant risk due to persistent anoxia at depth, such as in the Great Salt Lake (GSL), Utah, USA, which has elevated methyl mercury (40-90 ng/L) at depth, as well as elevated mercury in waterfowl in adjacent wetlands. Despite its inferred importance, the dynamics of salinity-driven density-stratified systems are not well characterized, particularly in terms of the impact to contaminant cycling. Dramatic decreases of methyl mercury in water and sediment in the GSL were previously reported in response to elimination of limited flow through the earthen railroad causeway separating the North and South Arms of the GSL in late 2013. Reopening of north-south flow in late 2016 offered the opportunity to understand the drivers of density stratification that in turn drive geochemical conditions supporting mercury methylation at depth. The evolution of density stratification following reopening of flow, and its impacts on aquatic chemistry in the midst of hydrologic forcings over larger timescales, demonstrated the relative impacts of engineered versus hydrologic (e.g., snowmelt runoff) forcings on stratification.

Measured aquatic chemistry parameters under destratified versus stratified conditions clarified the role of the deep brine layer versus underlying sediment organic matter in driving methyl mercury accumulation in the GSL. These findings from the Great Salt Lake demonstrate how forcings on stratification in endorheic lakes influence accumulation of toxic elements such as methyl mercury in bottom waters and underlying sediment.

### 3.2 Introduction

The Great Salt Lake (GSL), located in northwestern Utah, USA (Figure 3.1), is the largest terminal lake in the Western Hemisphere (Stephens et al., 1990). It is recognized as a site of hemispheric importance by the Western Hemisphere Shorebird Reserve Network, with over 1.4 million shorebirds using the GSL and surrounding wetlands for breeding and staging areas (Aldrich and Paul, 2002), and over seven million water birds utilizing the GSL and its associated wetlands during some portion of their biannual migration (Cline et al., 2011).

Elevated Hg concentrations in muscle from three GSL duck species (Cinnamon Teal, Northern Shoveler, Common Goldeneye) exceeded the EPA screening level of 0.3 mg/kg ww and resulted in a waterfowl consumption advisory (Scholl and Ball, 2005; Scholl and Ball, 2006), the only of its kind in the world. Elevated Se concentrations of liver that could result in sub-lethal toxic effects have been reported in 15% of Common Goldeneyes (Vest et al., 2009). However, interactions between selenium and mercury in wildlife may reduce their toxicity (Scheuhammer et al., 2007), and has been hypothesized as to why no reproductive impairment was observed in ducks at the GSL with elevated

burdens of both elements (Conover and Vest, 2009; Ohlendorf et al., 2009).

GSL South Arm saline waters support a limited but highly productive aquatic community and relatively simple food web, containing multiple species of phytoplankton, which are grazed by abundant of brine shrimp (*Artemia franciscana*) and brine flies (*Ephydria spp.*) (Belovsky et al., 2011). Brine shrimp and brine flies are fed upon by a large variety of migratory and resident birds (Wurtsbaugh et al., 2011). Brine shrimp are generally present as nauplii, juvenile, and adult from spring to fall; however, in winter when water temperatures are cold, cysts are the mean form of brine shrimp (Belovsky et al., 2011). Brine shrimp abundance is limited by phytoplankton abundance, which is depressed in winter time by shrimp grazing (Belovsky et al., 2011).

The construction of a railroad causeway in 1959 restricted flow between the North Arm (Gunnison Bay) and the South Arm (Gilbert Bay) of the GSL (Loving et al., 2000). Because more than 90% of the freshwater runoff enters the South Arm, the North Arm brine is concentrated by evaporation to be more saline (250–280 g/L) and denser than the South Arm brine (110–180 g/L) (Stephens et al., 1990, Gwynn, 2002). Limited flow of denser North Arm brine to the South Arm produces a persistent deep brine layer (DBL) underlying the shallow brine layer in the South Arm (Loving et al., 2000; Gwynn, 2002; Naftz et al., 2008). Recent elimination, followed by reestablishment, of flow between the North and South Arms in late 2013 and late 2016, respectively, destratified and then restratified the GSL (Yang et al., 2019).

Hg concentrations in the shallow brine layer do not exceed the EPA's aquatic life standard of 12 ng/L, whereas the DBL contains 30-80 ng/L (Naftz et al., 2008; Johnson et al., 2015, Valdes et al., 2017), with approximately half comprised of MeHg (Johnson et

al., 2015). Elevated Se and Hg concentrations in the DBL implicate it as a potential source of elevated contaminants in surrounding biota (Naftz et al., 2008; Vest et al., 2009; Wurtsbaugh et al., 2011; Saxton et al., 2013). Hg was speculated to be transferred from the DBL to shallow water by wind-driven mixing, and into the food chain via uptake by phytoplankton and benthic algae, which are then consumed by brine shrimp and brine flies that serve as diet for birds (Belovsky et al., 2011; Wurtsbaugh et al., 2011; Saxton et al., 2013; Jones and Wurtsbaugh, 2014). However, dramatic decreases in deep water THg and MeHg concentrations were not accompanied by decreased Hg concentrations in measured waterfowl (Valdes et al., 2017).

A linear relationship between Se concentrations in water and brine shrimp (beyond a threshold) was reported on the basis of field and laboratory observations (Brix et al., 2004). Se concentrations in brine shrimp, seston, and water from combined data sets from across the western U.S. (Byron et al., 2011) showed a significant and positive relationship between brine shrimp and water, and no relationship between seston and brine shrimp, or seston and water (Byron et al., 2011).

Although there has been considerable speculation regarding pathways by which Hg and Se enter GSL's ecosystem and food web, understanding is limited by a lack of frequent and co-located samples for water, biota, and other matrices. The goal of our study was to collect frequent, co-located samples of brine shrimp and surface and deep waters to determine whether their correspondence, or lack of, would implicate particular locations or phases as sources of the Hg and Se found in brine shrimp, a keystone species at the GSL.

### 3.3 Method

#### 3.3.1 Locations

During July 2016 to December 2017, water and brine shrimp from six sites in the South Arm (Gilbert Bay) of the GSL were analyzed for concentrations of THg, MeHg, and other trace elements (Figure 3.1). Both unfiltered and filtered (0.45 µm PES membrane) shallow waters (0.2 m below water surface) and deep waters (0.5 m above bottom) were collected. Samples were collected in triplicate. Water temperature and lake elevation were obtained from USGS data (USGS, 2018).

#### 3.3.2 Sampling and Analyses

##### 3.3.2.1 THg and MeHg

Clean hands–dirty hands protocol was followed during sample collection and analysis (US EPA, 1996). Unfiltered water samples were collected by peristaltic pump using acid-washed PTFE tubing into precleaned FLDPE and PTFE bottles that were pre-filled with trace metal grade (TMG) sulfuric acid to preserve samples with 0.5% acid. Filtered water samples were passed through 0.45 µm pore size, preacid-rinsed capsule filters (Geotech Environmental) in the field. All water samples were stored in the dark on ice in the field, refrigerated in the lab, and analyzed within 3 weeks of collection.

Water samples for HgT analysis were oxidized by amendment to 2-5% BrCl back in the lab. This higher BrCl concentration relative to established protocols was necessary to fully oxidize the high levels of sulfide and dissolved organic matter in some water samples (as described below). HgT concentrations in water were determined via reduction with SnCl<sub>2</sub>, purge and trap onto gold traps, thermal desorption, with

quantification by cold vapor atomic fluorescence spectroscopy (CVAFS) using a MERX-T automated system (Brooks Rand) using established techniques (US EPA, 2002). The USGS certified reference material (CRM) Hg64 for HgT in water was included in multiple analyzes, with recoveries averaging 85%. MeHg concentrations in water were measured after distillation with ammonium pyrrolidine dithiocarbamate (APDC), followed by aqueous-phase ethylation, purge and trap onto tenax traps, thermal desorption, pyrolytic decomposition, and CVAFS detection using a MERX-M automated system (Brooks Rand) using established techniques (US EPA, 2001).

### 3.3.2.2 Trace Elements

Water samples were collected and stored as described above into acid-washed LDPE bottles prefilled with sufficient TMG nitric acid to preserve samples to 3.3% acid. These samples were analyzed within 3 weeks of collection.

Samples were diluted 20-fold with ultrahigh purity water prior to analysis to reduce the salt interference, then were analyzed via inductively coupled plasma mass-spectrometry (ICP-MS) equipped with a collision/reaction cell (Agilent 7500ce) using established techniques (Carling et al., 2011). A calibrating solution containing all the elements reported was prepared gravimetrically using 1000 mg/L single-element standards (Inorganic Ventures, Inc.). This solution was used to prepare a calibration curve with six points plus a blank. Detection limit (DL) was determined as three times the standard deviation of the all blanks analyzed throughout the run. A continuing calibration verification solution was prepared using NIST SRM 1643e. This solution was diluted by a factor of 20 and analyzed as a sample between each 4 samples during each run. The

agreement between measured and calculated values was better than 10% for all elements with the exception of Fe, which had a measured value up to ~20% larger than calculated. Also, matrix spikes were analyzed for synthetic GSL water and GSL brine samples. For simulated GSL waters, averaging spike recovery rates were  $103\% \pm 2\%$  for Cu,  $106\% \pm 5\%$  for Zn,  $80\% \pm 5\%$  for Cd,  $75\% \pm 2\%$  for As,  $73\% \pm 4\%$  for Se, and  $81\% \pm 6\%$  for Pb; For GSL brine samples, averaging spike recovery rates were  $114\% \pm 9\%$  for Cu,  $89\% \pm 7\%$  for As,  $63\% \pm 7\%$  for Se, and  $61\% \pm 1\%$  for Pb (Appendix B). Field process blanks yielded values below or near detection limits for all elements.

### 3.3.2.3 Brine Shrimp

Brine shrimp were collected using a tow net with a mesh size of 150-200  $\mu\text{m}$ , then transferred to acid-washed PE bottles and placed on ice in the field. Once in the lab the same evening, samples were thoroughly rinsed with UHP water to remove brine and detritus, while larger foreign material was removed manually with plastic tweezers. Samples were then frozen, freeze dried, and homogenized.

Brine shrimp samples were microwave digested in a 2:1 mixture of  $\text{HNO}_3:\text{H}_2\text{SO}_4$  (TMG). Specifics of the microwave digestion can be found in the supplementary info. Digested samples were diluted 5-fold with UHP water, then split with part of the sampling being amended to 2% BrCl for HgT analysis, while the remaining sample was diluted an additional 7-fold for trace element analysis with a quadruple ICP-MS equipped with a collision cell (Agilent 7900) and the use of six internal standards.

### 3.3.2.4 Bioaccumulation Factors (BAF)

BAFs were calculated for spatially and temporally collocated brine shrimp and both shallow and deep filtered water samples as follows:

$$BAF = \frac{C_{BS}}{C_{FW}}$$

where, BAF is the bioaccumulation factor (L/Kg), CBS is the trace element concentrations in brine shrimp (mg/Kg, dw), and CFW is the trace element concentrations in filtered water (mg/L).

## 3.4 Results

Se concentrations in brine shrimp and water varied dramatically (factor of 4) over monthly intervals (Figure 3.2). Temporal trends in Se concentrations were similar across all sites for both water and brine shrimp (Figure 3.2). Temporal variability in Se was much greater than spatial variability, with spatial variability in Se concentrations being less in brine shrimp than water (Figure 3.2). Temporal correspondence of Se concentrations between brine shrimp and water was evident (Figure 3.2). This correlation applied to all water samples as there was very little difference between the concentrations of Se in filtered or unfiltered waters or between surface or deep waters during this time (Figure 3.2). Se was predominantly found in the dissolved phase (> 90%) (Appendix B). There were no clear seasonal trends in the Se concentrations in water or brine shrimp that were consistent across years. In August 2016, the southern sites (3510, GB14, and 4069) had higher concentrations of Se in water and brine shrimp, but such a trend did not exist during the rest of the sampling period (Figure 3.2).

In contrast to Se, THg concentrations in brine shrimp showed temporal

correspondence with shallow filtered water only (Figure 3.3). No temporal correspondence in THg concentrations was observed between brine shrimp and unfiltered shallow water or deep waters (filtered and unfiltered) (Figure 3.3). THg concentrations were approximately 2.1- and 1.6-fold higher in deep waters relative to shallow waters for filtered and unfiltered water, respectively (Figure 3.3). THg was relatively evenly distributed between the dissolved and particulate phases, with dissolved comprising ~ 64% and 65% for shallow and deep waters, respectively (Appendix B), and concentrations of THg in unfiltered waters were roughly 0.7- and 0.4-fold higher than in filtered waters for shallow and deep water, respectively (Figure 3.3). There was a strong seasonal signal in THg in brine shrimp and shallow waters, with the lowest concentrations in the spring and fall and an annual maximum each summer (Figure 3.4). This trend was not present in THg in deep waters or unfiltered surface waters (Figure 3.4). Temporal variability in THg concentrations was notably greater than spatial variability for both brine shrimp and surface waters (Figure 3.3). However, both spatial and temporal variability were greater in THg concentrations in deep relative to shallow water, which was driven by anoxic events in deep waters in 2017 (Yang et al., 2019).

MeHg concentrations in water were not correlated with THg concentrations in brine shrimp (Appendix B) despite MeHg comprising approximately 90% of THg concentration in brine shrimp. Average MeHg:THg in brine shrimp was equal to 89% (ranging 77-105%) in 2016, 89% (ranging 75-102%) in 2017, and 87% (ranging 68-106%) in 2018 (Appendix B). Lack of correspondence between MeHg concentration in shallow water with THg concentration in brine shrimp despite co-occurrence of elevated concentrations of both MeHg and THg in deep waters (Appendix B) further indicates lack

of direct impact of deep waters, and may reflect the impact of transport processes as well as transformation (e.g., demethylation) in the shallow water column (Yang et al., 2019).

Concentrations of other trace elements (e.g., Cr, Co, As, Zn, Fe, Mn, Cu, and Pb) displayed no correspondence between brine shrimp and water (Appendix B). However, concentrations of many trace elements in brine shrimp exhibited clear seasonal trends, which were not present in surface or deep waters (Appendix B).

### 3.5 Discussion

#### 3.5.1 Seasonality

THg concentrations in brine shrimp and filtered shallow water were not only temporally correlated, but also exhibited clear seasonal trends that were consistent across years. HgT concentrations in both brine shrimp and filtered surface waters were elevated in summer (Figures 3.4a and 3.4d), which was observed previously by Naftz et al. (2008) who did not have sufficient temporal frequency in observations to describe the complete nature of annual seasonality demonstrated by our data set. The increase in THg concentrations in brine shrimp each spring coincided with the increase in HgT in surface waters, as well as with increased water temperature, increased lake stage, decreased salinity, increased dissolved organic nitrogen, decreased phytoplankton abundance and chlorophyll A concentration, shift in phytoplankton community to more *Cyanophytes* but fewer *Chlorophytes* and *Bacillariophytes*, increased brine shrimp abundance, and an aging brine shrimp population (from nauplii to juveniles to adults) (Belovsky et al., 2011 and Appendix B). Thus, the observed seasonal pattern in HgT in brine shrimp likely reflects a combination of (1) the bioavailability of Hg in surface waters, either to the

brine shrimp themselves or their phytoplankton prey, (2) shift in the phytoplankton community and seston of the GSL that the brine shrimp filter feed, and (3) seasonal changes in brine shrimp development and metabolism. While we did not monitor changes in the phytoplankton community composition or the concentration of THg in the phytoplankton, the strong correspondence between concentrations of THg in filtered surface waters and brine shrimp suggests this is an important factor controlling uptake of Hg into the GSL foodweb.

Unlike THg, Se concentrations in brine shrimp and filtered shallow water, while temporally correspondent (Figure 3.2), did not show seasonality that was repeated from year to year (Figures 3.4b and 3.4e). The correspondence among brine shrimp and aqueous Se concentrations is in agreement with Brix et al. (2004), Byron et al. (2011), and Adams et al. (2015). Whereas the latter study also concerned field measurements, their water and brine shrimp samples were not always coincident in time, and so their observations did not elucidate the temporal correspondence we describe above.

Lack of predictable seasonality in Se concentrations may have been driven by year-to-year variability in Se input and output fluxes (e.g., Diaz et al., 2008). Inputs are primarily runoff, and outputs primarily include sedimentation and volatilization (Diaz et al., 2009), all of which are related to weather and climate via snowpack, wind, and temperature (Amouroux and Donard, 1996; Diaz et al., 2009).

Notably, Se concentrations in water described here ranged approximately a factor of ten higher relative to those reported a decade earlier (approximately 0.6 ug/L) (Diaz et al., 2009) (Appendix B). Whether the more recent higher values (Figures 3.2 and Appendix B) reflect an extension of the upward trend reported a decade ago (Diaz et al.,

2009) is unclear and worthy of further investigation.

Some of the elements for which temporal correspondence between brine shrimp and water was absent (Cr, Co, Fe, Pb, V, Th, and U) showed seasonality that was repeated from year to year in brine shrimp but not in water, as exemplified by Cr in brine shrimp (Figure 3.4c) and water (Figure 3.4f).

### 3.5.2 Partitioning

Bioaccumulation factors (BAF) for distribution of Se between shallow filtered water and brine shrimp ranged from 300 to 3000 L/kg (Figure 3.5a), which is similar to, but somewhat lower than, that previously reported for the GSL (1,000 to 20,000 L/kg) (Adams et al., 2015) and for the marine water (3,947, to 145,455 L/Kg) (DeForest et al., 2007). This was because the Se concentrations in GSL water increased approximately one order of magnitude in past decades (from ~0.2ug/L to ~4ug/L) (Appendix B), whereas the Se concentrations in brine shrimp were relatively constant (~4000 ng/g dw.) (Adams et al., 2015). BAFs for Se in brine shrimp were negatively correlated with the Se concentration in filtered shallow water ( $P < 0.05$ ) (Figure 3.5a), consistent with the same inverse relationship reported in other studies (McGeer et al., 2003; DeForest et al. 2007; Adams et al., 2015), indicating that Se uptake is limited at higher dissolved Se concentrations. Values for the BAF for THg distribution between brine shrimp and shallow filtered water ranged between 150,000 to 500,000 L/kg (Figure 3.5b) within the range of BAF that previously reported for marine water (57,094 to 3,899,000 L/Kg) (DeForest et al. 2007), and showed no correlation with the concentration of THg in filtered shallow water (Figure 3.5b).

Molar ratios of Se:Hg in brine shrimp were approximately  $20 \pm 15$  (ranging 6 to 75) (Appendix B), indicating that simple complexes such as HgSe may not have been responsible for lack of toxic outcomes, or that Se is far in excess of Hg to produce antagonistic avoidance of toxicities.

### 3.5.3 Pathways to Biota

For the first time, correspondence between THg concentrations in brine shrimp and a specific water column phase, i.e. dissolved THg in surface waters, has been established at GSL (Figure 3.3). Past studies have highlighted the DBL and its very high concentrations of MeHg and THg as a potential reservoir from which mercury may propagate into the surrounding ecosystem (Naftz et al., 2008; Vest et al., 2009; Wurtsbaugh et al., 2011; Saxton et al., 2013). This transfer pathway was inferred by Johnson et al. (2015) based on the temporal correspondence of decreased inorganic Hg methylation rate in the DBL and reduced Hg burdens among brine shrimp and brine flies. However, Valdes et al., (2017) found that dramatic reductions in THg and MeHg deep water concentrations following destratification and disappearance of the DBL did not result in a decrease in THg in multiple species of waterfowl or brine flies sampled during that period. The above observations do not indicate a connection between elevated THg and MeHg in the DBL and elevated Hg in GSL biota, and our finding that THg in brine shrimp and dissolved THg in surface waters correspond temporally (seasonally) suggests that any potential influence of the DBL occurs via the shallow water column.

The strong temporal correspondence between THg concentrations in brine shrimp and shallow filtered water (Figure 3.3) may be expected given that the brine shrimp life

cycle is lived within the shallow water column, as well as by the observation that mercury bound in dissolved complexes and in the nanoparticulate fraction that would have passed through the filters we used tend to be more bioavailable than particulate species (Hsu-Kim et al., 2013). The lack of temporal correspondence between brine shrimp and shallow unfiltered water (Figure 3.3) suggests that particle-bound THg is less bioavailable to brine shrimp relative to dissolved (filterable) Hg. Previous lab studies have suggested that brine shrimp may preferentially feed near the interface between the upper brine and deep brine layers, and thus that the DBL may be an important source of Hg to the brine shrimp diet (Jones and Wurtzbaugh, 2014). However, our field results show no significant temporal correspondence between concentrations of THg in brine shrimp and deep waters (filtered and unfiltered) (Figure 3.3). Similarly, we found no correlation between HgT in brine shrimp and concentrations of MeHg in shallow or deep waters (filtered or unfiltered), despite MeHg being the most bioavailable and more readily bioaccumulated form of Hg in most aquatic ecosystems (Watras and Bloom, 1992; Mason et al., 1996; Wang and Wong, 2003; Pickhardt and Fisher, 2007), and given that on average, 89% of the mercury in brine shrimp is MeHg (as measured in a biannual subset of our samples). We speculate that the correlation between THg in brine shrimp and filtered surface waters may be related to previous observations that inorganic mercury inputs to aquatic ecosystems via recent atmospheric deposition tend to be more bioavailable and readily methylated than other internal or external sources of inorganic mercury (Hammerschmidt and Fitzgerald, 2006; Orihel et al., 2006, 2007; Paterson et al., 2006; Harris et al., 2007) and given that atmospheric deposition has been estimated to be the largest contemporary input of mercury to the GSL (Naftz et al., 2009). Because the

vast majority of the Hg in brine shrimp is MeHg, this would require that prior to MeHg uptake by brine shrimp (either directly or through their phytoplankton prey) atmospherically deposited inorganic mercury be first methylated, possibly in surficial sediment underlying the oxic upper brine, and not in the DBL or sediments underlying the DBL as previously suggested. However, the reasons for the lack of a correlation between MeHg in surface waters and brine shrimp remain unclear. Additional evidence suggesting that deep water is not the primary source of Hg in brine shrimp is that temporary increases in THg concentrations in deep waters (filtered and unfiltered) at site 3510 during spring and fall of 2017 (Figure 3.3) were not reflected in brine shrimp, but were coincident with temporarily decreased dissolved oxygen (DO) and increased sulfide in those deep waters (Yang et al., 2019).

Our results show that concentrations of many trace elements vary substantially temporally and display strong seasonal trends such that annual or biannual sampling may not reveal the actual range of concentrations in water or biota, unless they serendipitously occur during annual minima and maxima. Similarly, efforts to detect long-term changes in elemental concentrations in GSL water or biota must account for the dramatic seasonal changes exhibited by these trace elements. Whereas bioconcentrated elements such as Hg may show consistent year-to-year minima and maxima, Se does not, requiring frequent sampling to capture the unpredictable dynamic of Se.

### 3.6 Acknowledgement

This research was supported by funding from the Utah Divisions of Forestry, Fire, and State Lands (FFSL) of the Utah Department of Natural Resource (180608) program

from Utah Division of Water Quality, and the National Science Foundation Low Temperature Geochemistry and Geobiology Program (EAR 1637196). Any opinions, findings, and conclusions or recommendations expressed in this material are those of the authors and do not necessarily reflect the views of the FFSL, Utah Division of Water Quality, and National Science Foundation.

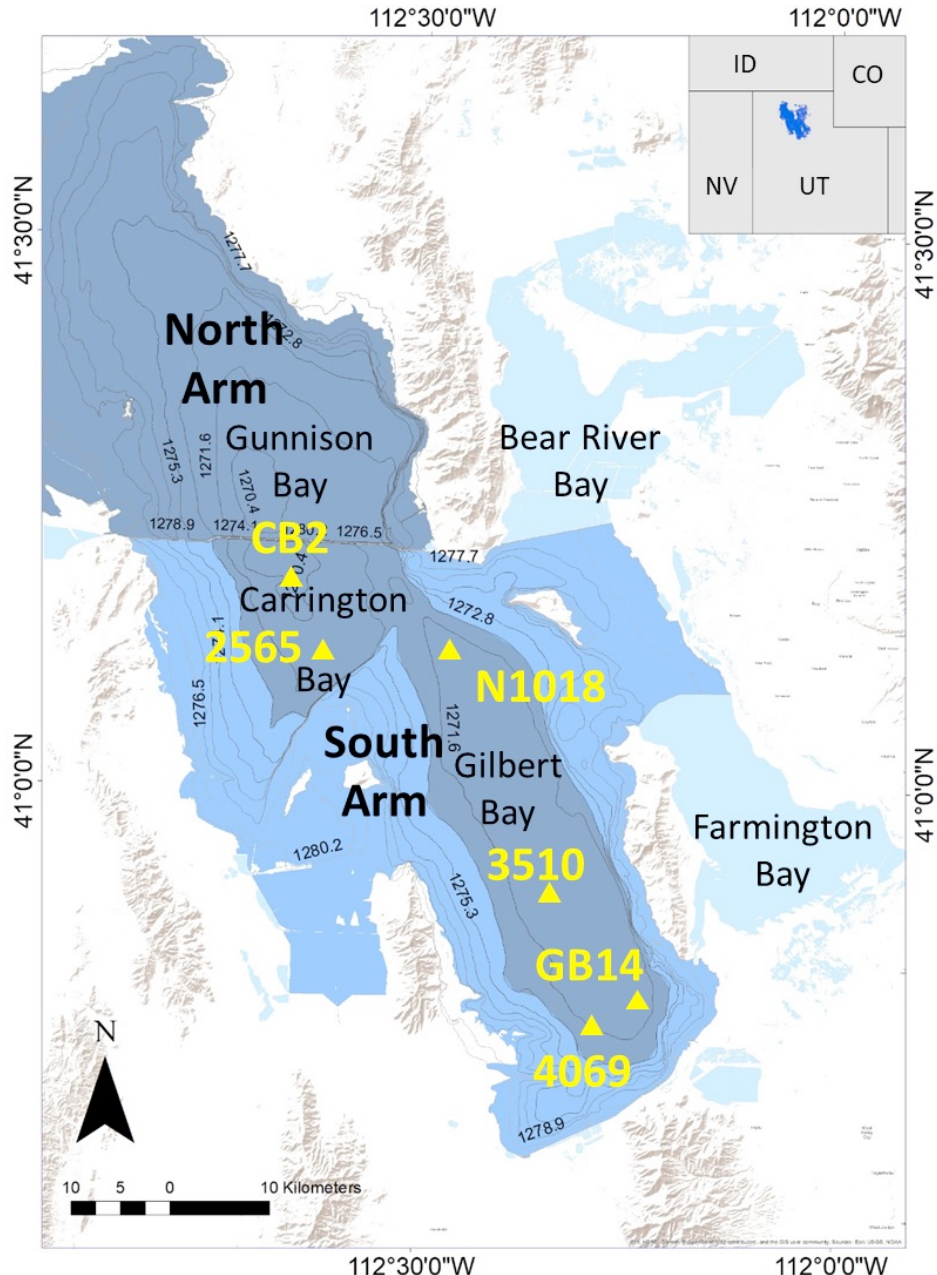


**Figure 3.1.** The Great Salt Lake with sample sites. Triangles represent the sample locations collected from 2006 to 2018. Contour intervals represent elevation above MSE in meters. Shading represents typical water salinities (% total dissolved solids) of deep waters during 2007-2012, with gray corresponding to approximately 28%, dark blue corresponding to approximately 15%, and the light blue representing salinities less than 5%. Thus, the darker shading in the South Arm indicates the approximate extent of the deep brine layer until 2012.

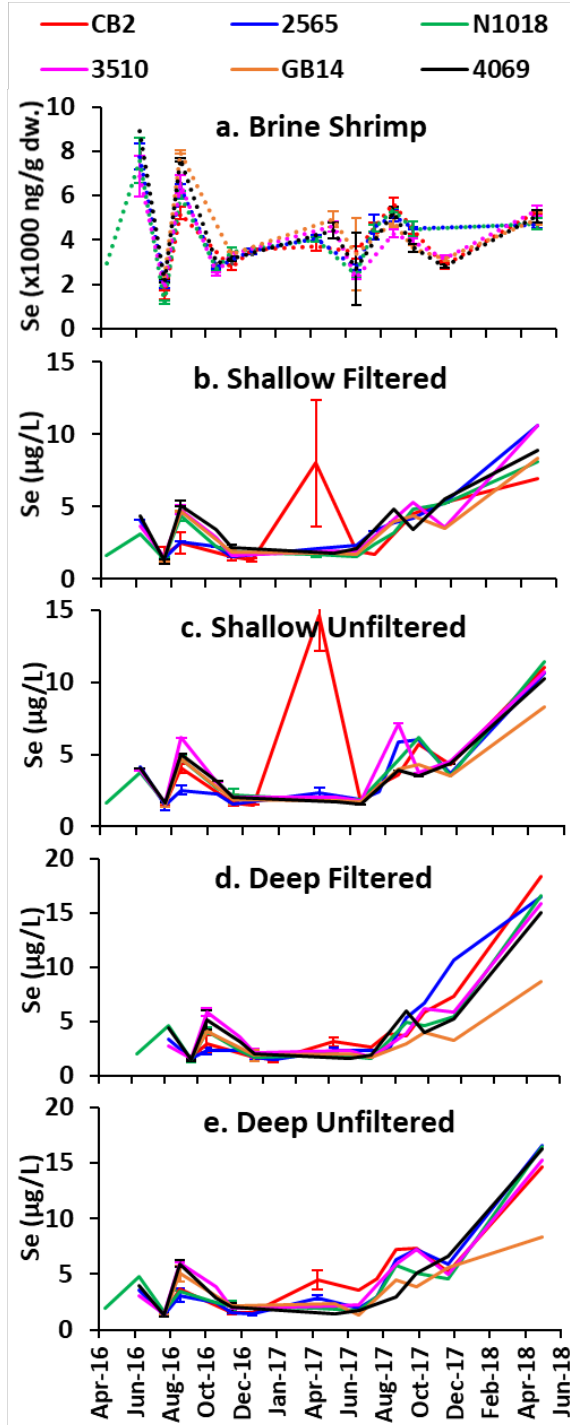


**Figure 3.2.** Se concentrations in a) brine shrimp, b) shallow filtered water, c) shallow unfiltered water, d) deep filtered water, and e) deep unfiltered water at six sites (denoted by color) across GSL. Dotted lines represent concentrations in brine shrimp, solid lines represent concentrations in water. The highest value at CB2 in shallow unfiltered was 14.7 µg/L.

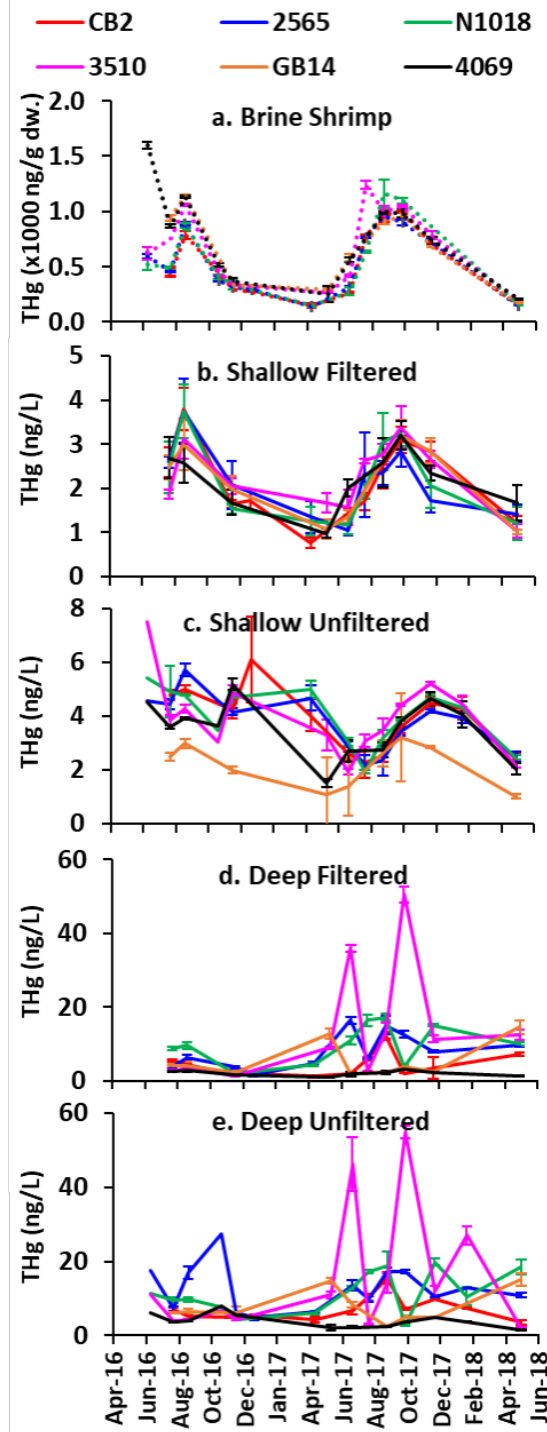


**Figure 3.3.** THg concentrations in a) brine shrimp, b) shallow filtered water, c) shallow unfiltered water, d) deep filtered water, and e) deep unfiltered water at six sites (denoted by color) across GSL. Dotted lines represent concentrations in brine shrimp, solid lines represent concentrations in water.

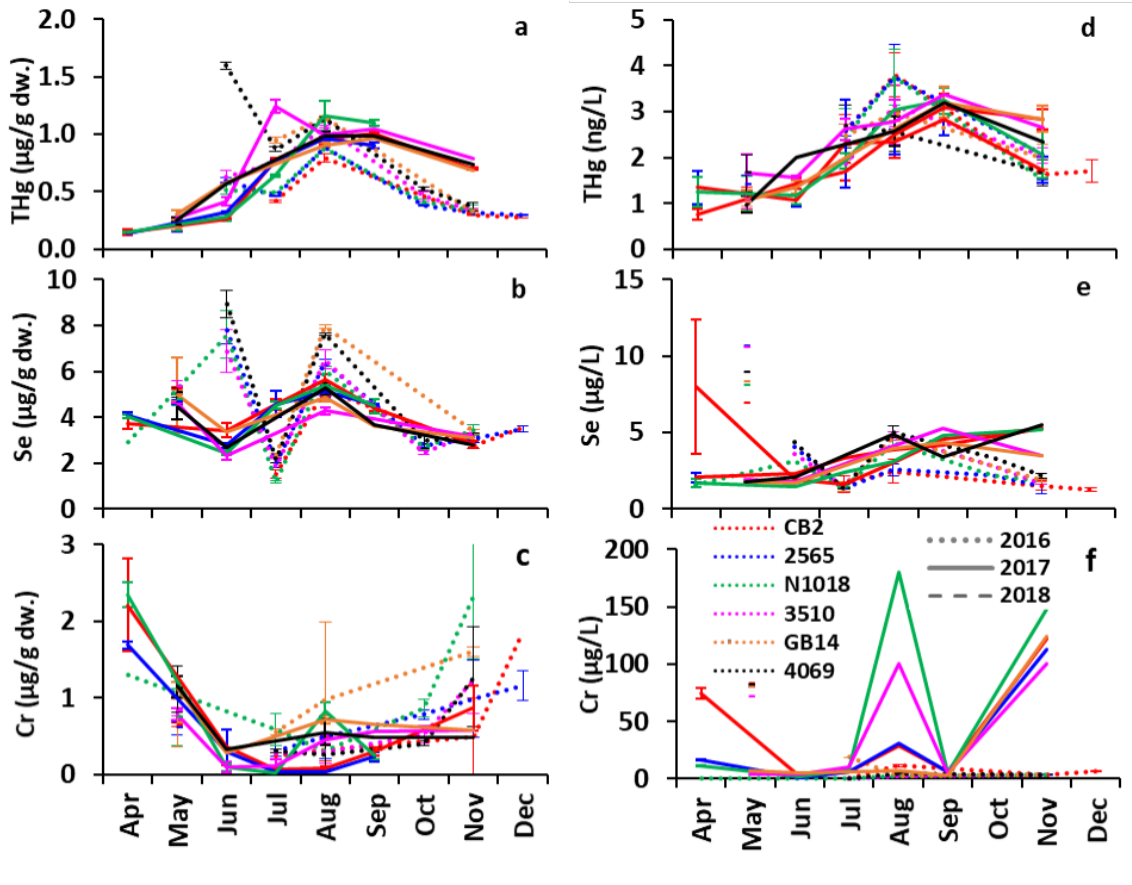


**Figure 3.4.** Trace element concentrations seasonal variation in brine shrimp (left column) for a) THg, b) Se, and c) Cr, and in shallow filtered water (right column) for d) THg, e) Se, and f) Cr at six site (denoted by color) across GSL from April to December in 2016 and 2017 (dotted line and dashed line, representatively).

## CHAPTER 4

### CONCLUSION

Two kinds of perturbation occurred in GSL, one being persistent brine/brine stratification generated by denser brine flow from the North Arm, the other being temporal freshwater/brine stratifications produced by snowmelt runoff. Elevated concentrations of sulfide, MeHg, and THg in deep water in response to both temporal and persistent stratification highlighted the role of organic matter in underlying sediment in GSL, and elucidated the potential role of DBL as a sort of cap that promotes the accumulation of MeHg and organic matter at depth. Underlying sediment was implicated responsible for greater MeHg cumulative flux into the system, and possible diffusive transfer of MeHg from DBL to UBL was suggested. Further understanding of MeHg source and pathway will benefit from the development of a hydrodynamic model of DBL in GSL.

Temporal correspondence of Se and Hg between water and brine shrimp, especially relative strong correspondence with shallow filtered water, indicated that both elements transfer to biota via shallow water in dissolved phase. For Se, transfer occurred predominately directly from water rather than through phytoplankton and benthic detritus, emphasizing the importance of monitoring Se concentrations in water. Whereas the bioaccumulation of Se and Hg did not affect partitioning to particulate phase, the

uptake mechanism was possibly overwhelmed above some threshold concentrations of dissolved concentrations. Additionally, temporal variation of trace element concentrations highlighted the importance of sampling time and frequency for understanding the actual range in water and biota. The unpredictable dynamic of Se requires frequent sampling relative to Hg, which showed year-to-year repeatable maxima and minima.

## **APPENDIX A**

### **SUPPORTING INFORMATION FOR CHAPTER 2**

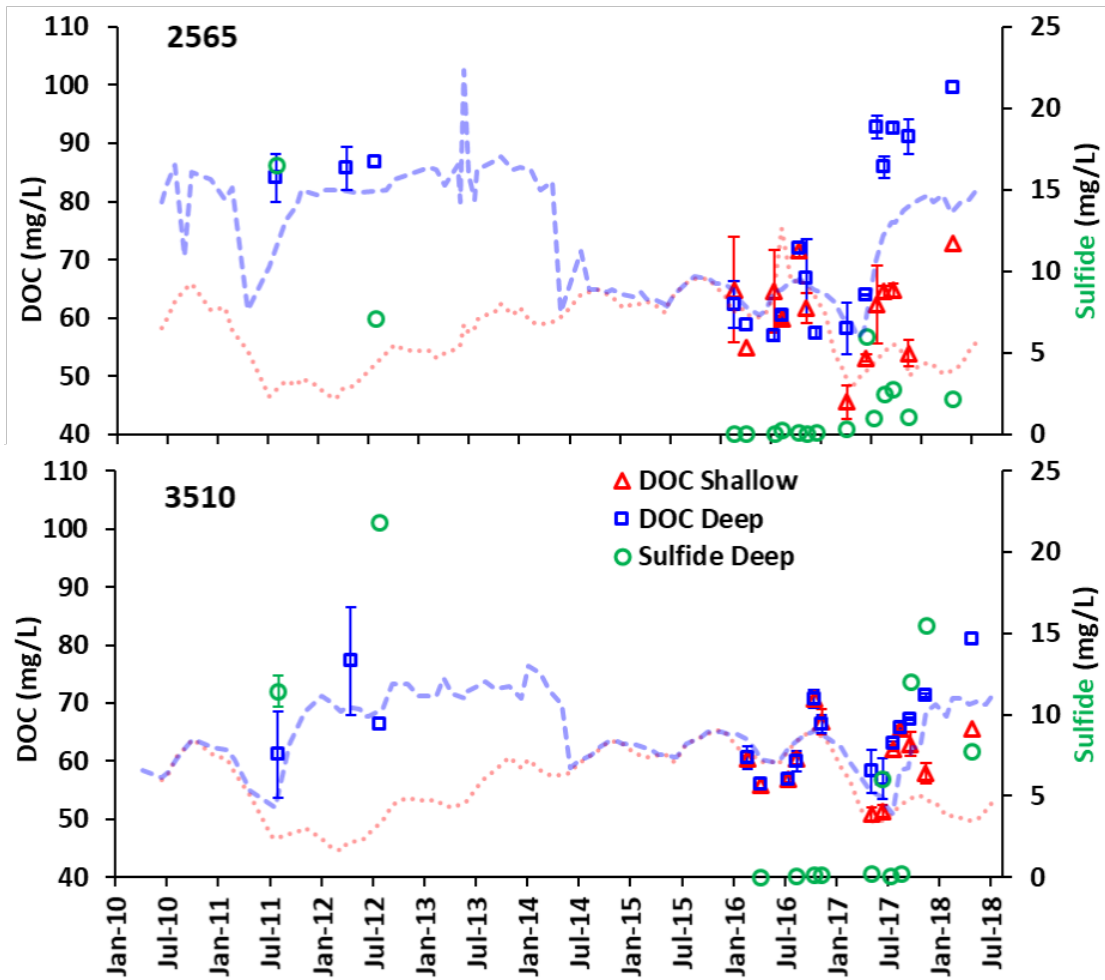


Figure A1. DOC in shallow and deep water, and dissolved sulfide ( $S^{2-}$ ) concentrations in deep waters, as well as densities of shallow and deep waters (dotted and dashes lines, respectively) at site 2565 and 3510 from 2010 to 2018. Sulfide concentrations lower than the detection limit (0.02 mg/L) are plotted as 0.01 mg/L. Sulfide and DOC data were not collected during 2013-2016. Sulfate data were not collected during 2014-2016. Density scale omitted for simplicity, see Figure 2.2.

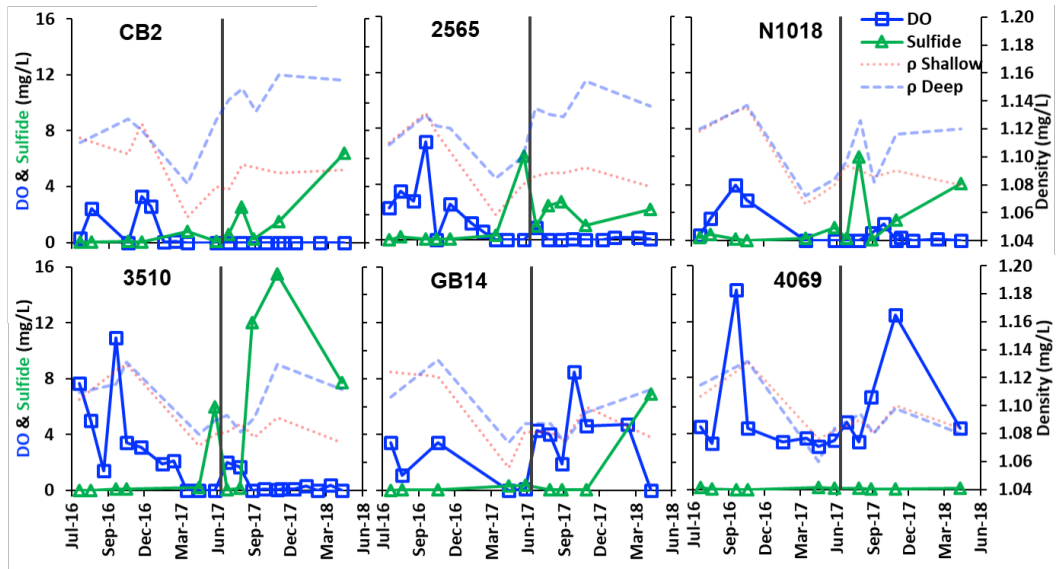


Figure A2. Deep water (0.5 m above bottom) dissolved oxygen (DO) concentration and densities of shallow (0.2 m below water surface) and deep water at six sites across Great Salt Lake. Figure panels are ordered from northernmost site (CB2) to southernmost site (4069). Grey vertical bars represent the timing the first N-to-S flow through new breach was monitored (July 2017).

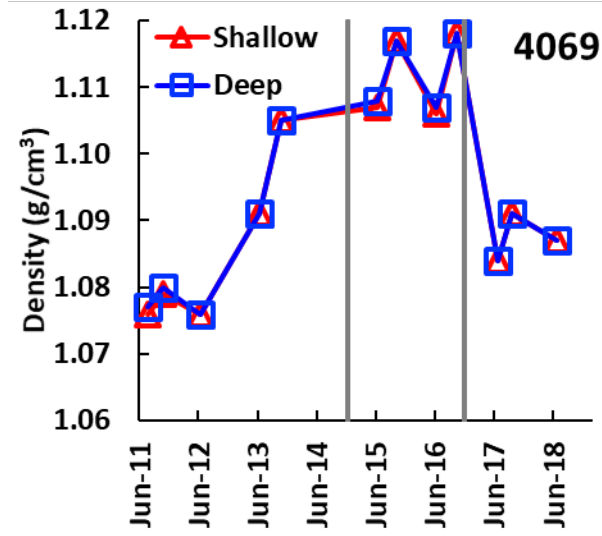


Figure A3. Shallow and deep water column densities at site 4069 with time. Grey vertical bars represent the time of railroad causeway culvert closure (left bar, Dec 2013) and reopening (right bar, Dec 2016).

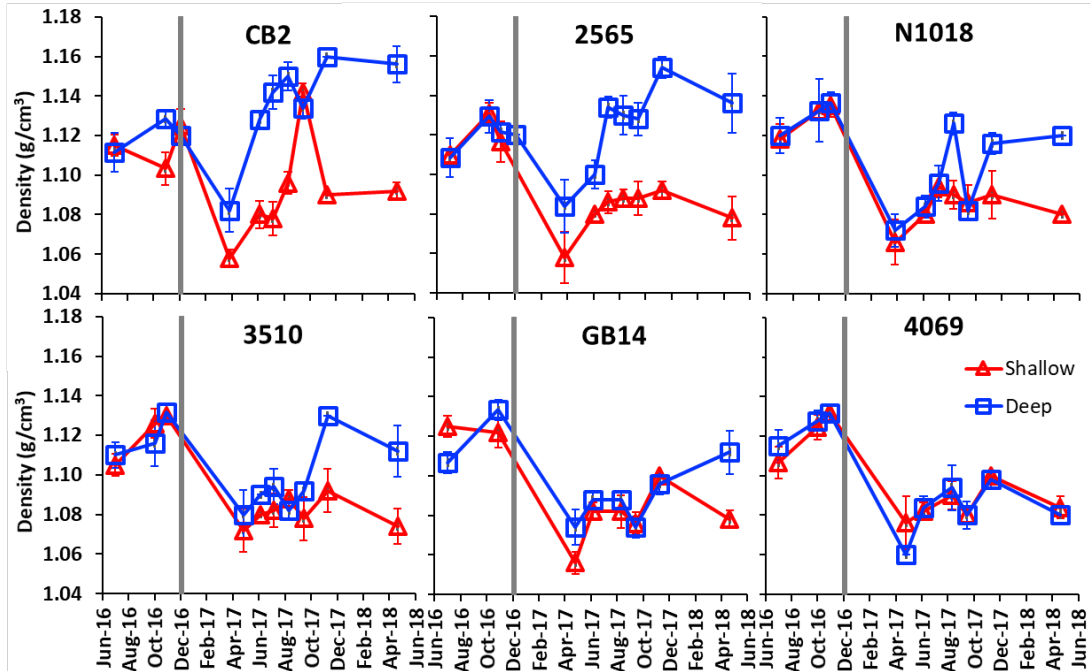


Figure A4. The densities (average  $\pm$  standard deviation) for shallow (0.2m below surface) and deep (0.5m above bottom) water column at six sites across Great Salt Lake. Northern sites (CB2, 2565) at left top, southern sites (3510, GB14 and 4069) at bottom with intermediate sites (N1018) at left top. Grey vertical bars represent the time of causeway culvert reopening (December, 2016).

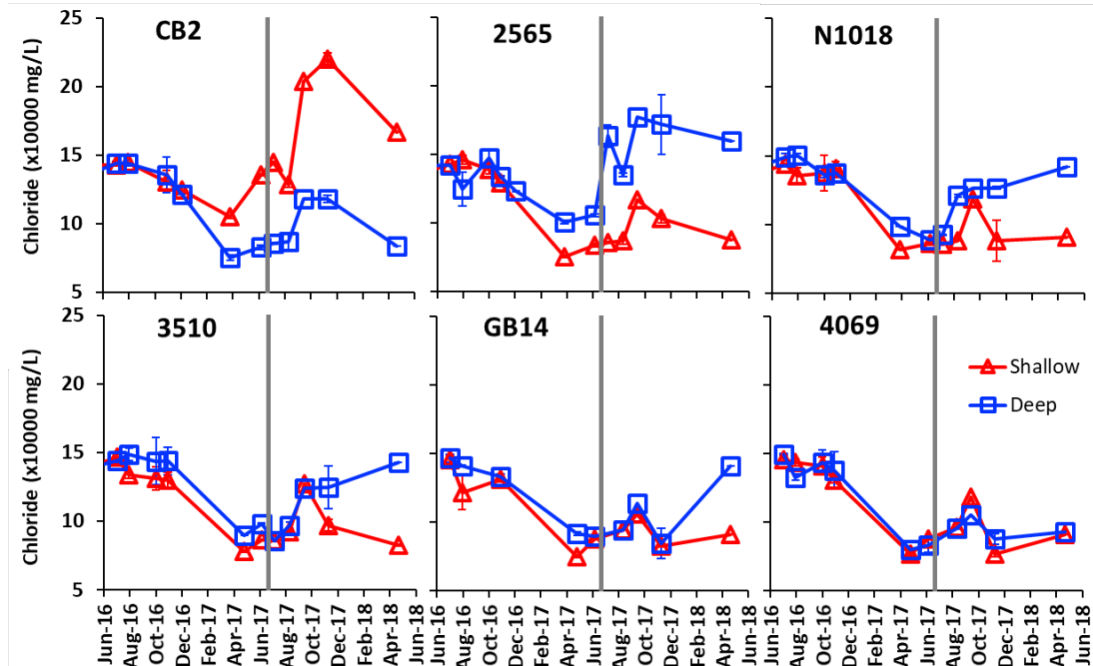


Figure A5. Filtered chloride concentration (mean  $\pm$  standard deviation) of shallow (0.2 m below water surface) and deep water at six sites across Great Salt Lake. Figure panels are ordered from northernmost site (CB2) to southernmost site (4069). Grey vertical bars represent the timing the first N-to-S flow through new breach was monitored (July 2017).

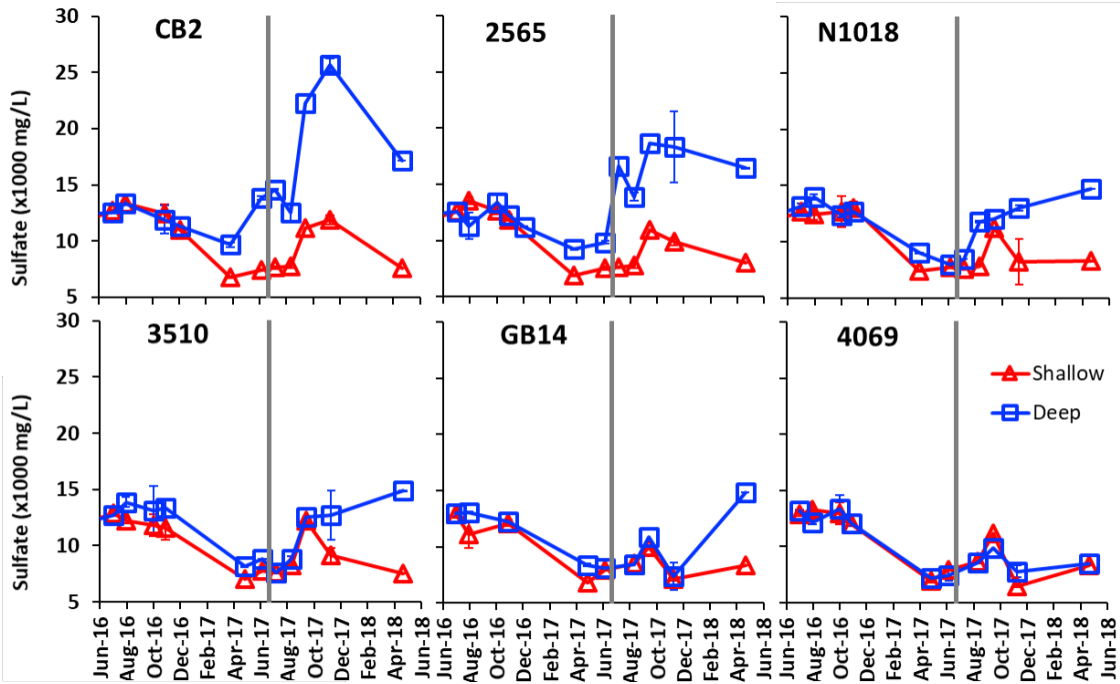


Figure A6. Filtered sulfate concentration (mean  $\pm$  standard deviation) of shallow (0.2 m below water surface) and deep water at six sites across Great Salt Lake. Figure panels are ordered from northernmost site (CB2) to southernmost site (4069). Grey vertical bars represent the timing the first N-to-S flow through new breach was monitored (July 2017).

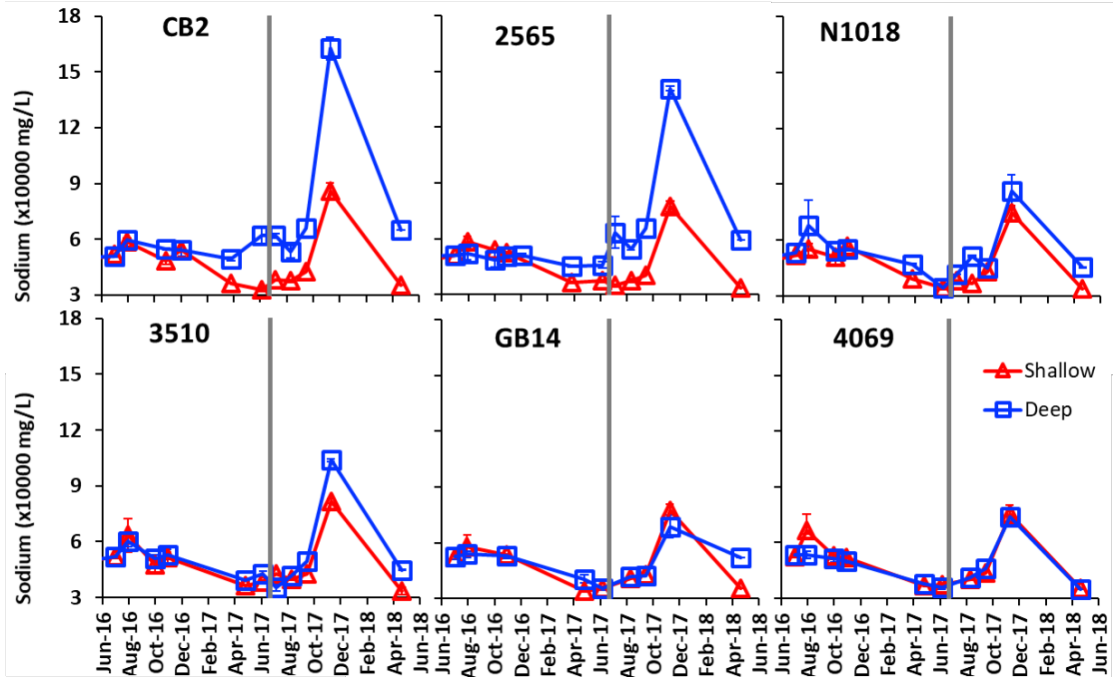


Figure A7. Filtered sodium concentration (mean  $\pm$  standard deviation) of shallow (0.2 m below water surface) and deep water at six sites across Great Salt Lake. Figure panels are ordered from northernmost site (CB2) to southernmost site (4069). Grey vertical bars represent the timing the first N-to-S flow through new breach was monitored (July 2017).

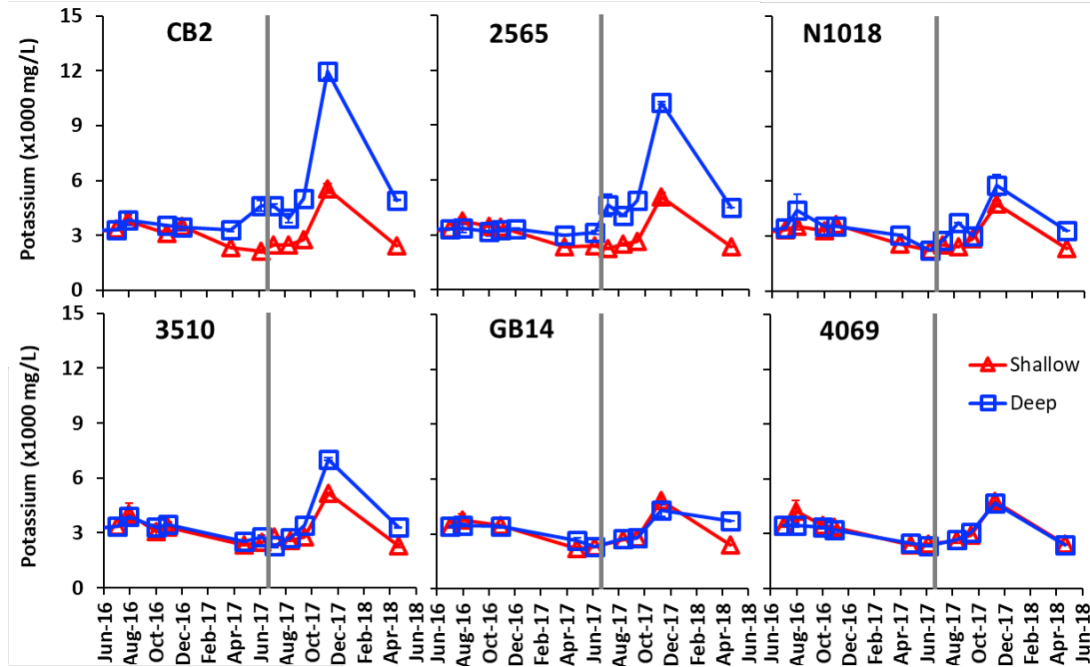


Figure A8. Filtered potassium concentration (mean  $\pm$  standard deviation) of shallow (0.2 m below water surface) and deep water at six sites across Great Salt Lake. Figure panels are ordered from northernmost site (CB2) to southernmost site (4069). Grey vertical bars represent the timing the first N-to-S flow through new breach was monitored (July 2017).

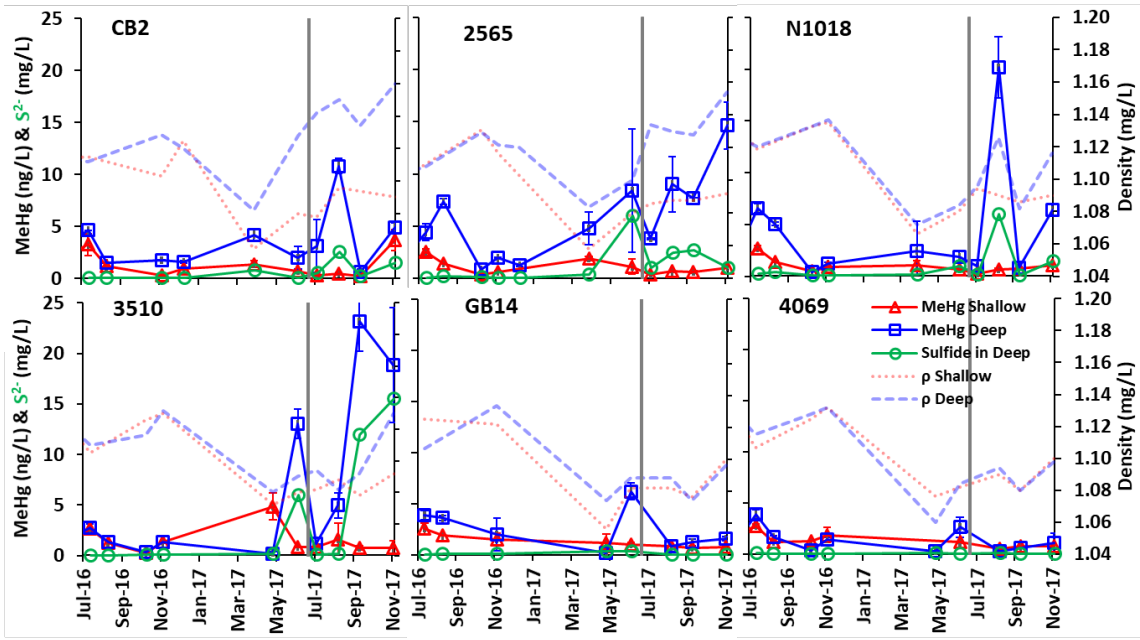


Figure A9. Deep water (0.5 m above bottom) sulfide ( $S^{2-}$ ) concentration, unfiltered MeHg concentrations and densities of shallow (0.2 m below water surface) and deep water at six sites across Great Salt Lake. Figure panels are ordered from northernmost site (CB2) to southernmost site (4069).

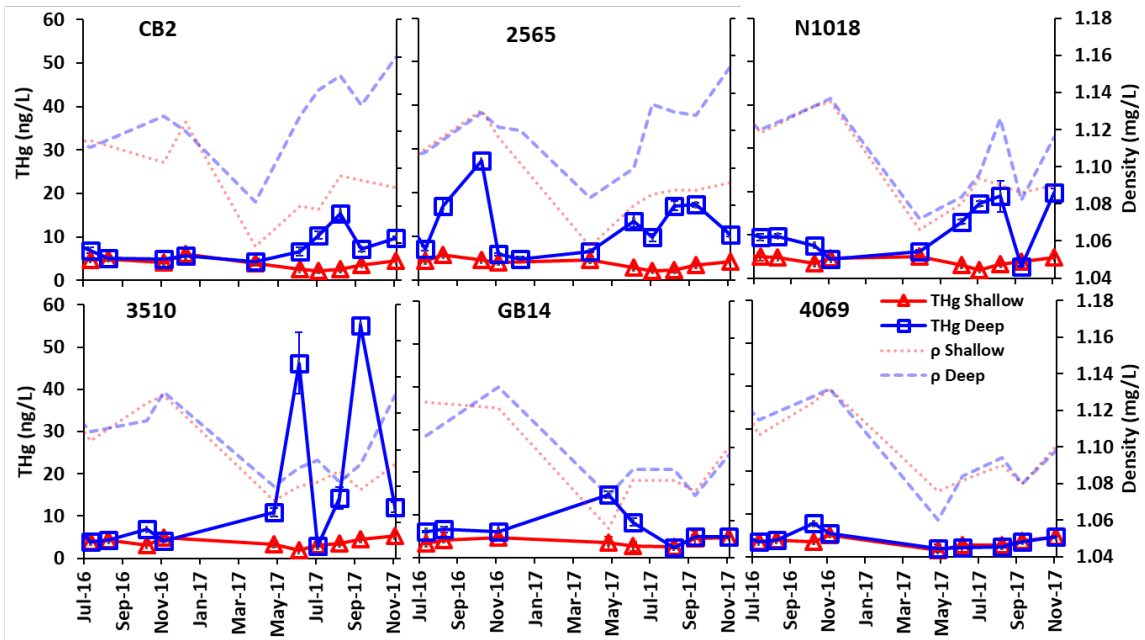


Figure A10. Unfiltered THg concentration (mean  $\pm$  standard deviation) and densities of shallow (0.2 m below water surface) and deep water at six sites across Great Salt Lake. Figure panels are ordered from northernmost site (CB2) to southernmost site (4069).

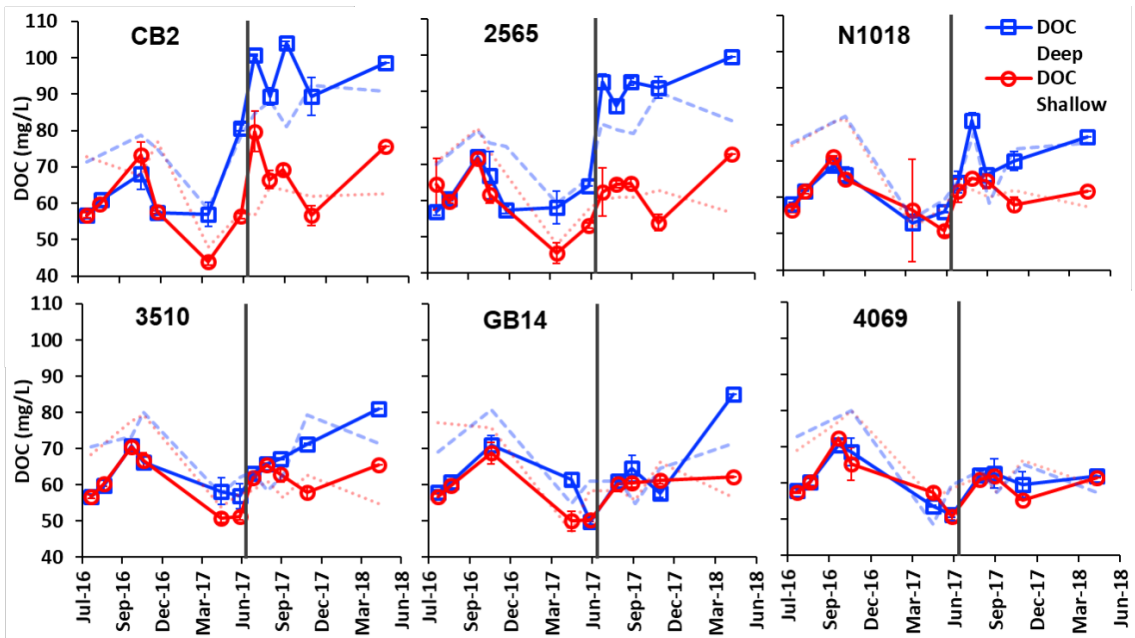


Figure A11. DOC concentration (mean  $\pm$  standard deviation) and density of shallow (0.2 m below water surface) and deep water at six sites across Great Salt Lake. Figure panels are ordered from northernmost site (CB2) to southernmost site (4069). Grey vertical bars represent the timing the first N-to-S flow through new breach was monitored (July 2017). Density scale omitted for simplicity.

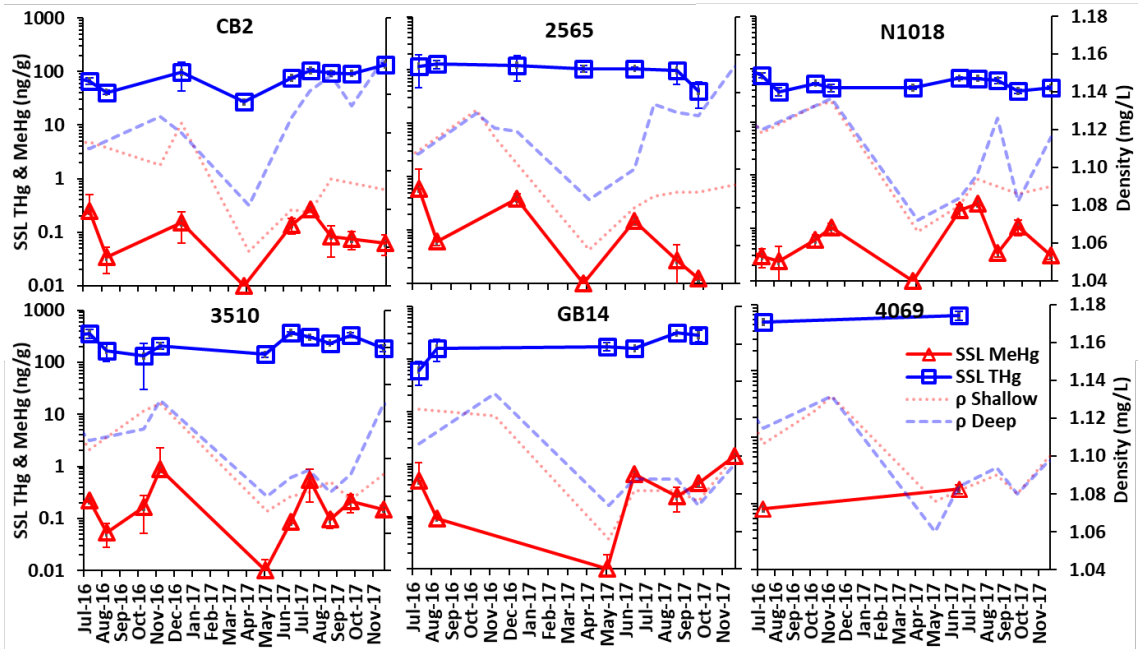


Figure A12. THg and MeHg concentrations for SSL, as well as densities of shallow (0.2 m below water surface) and deep water at six sites across Great Salt Lake. Figure panels are ordered from northernmost site (CB2) to southernmost site (4069).

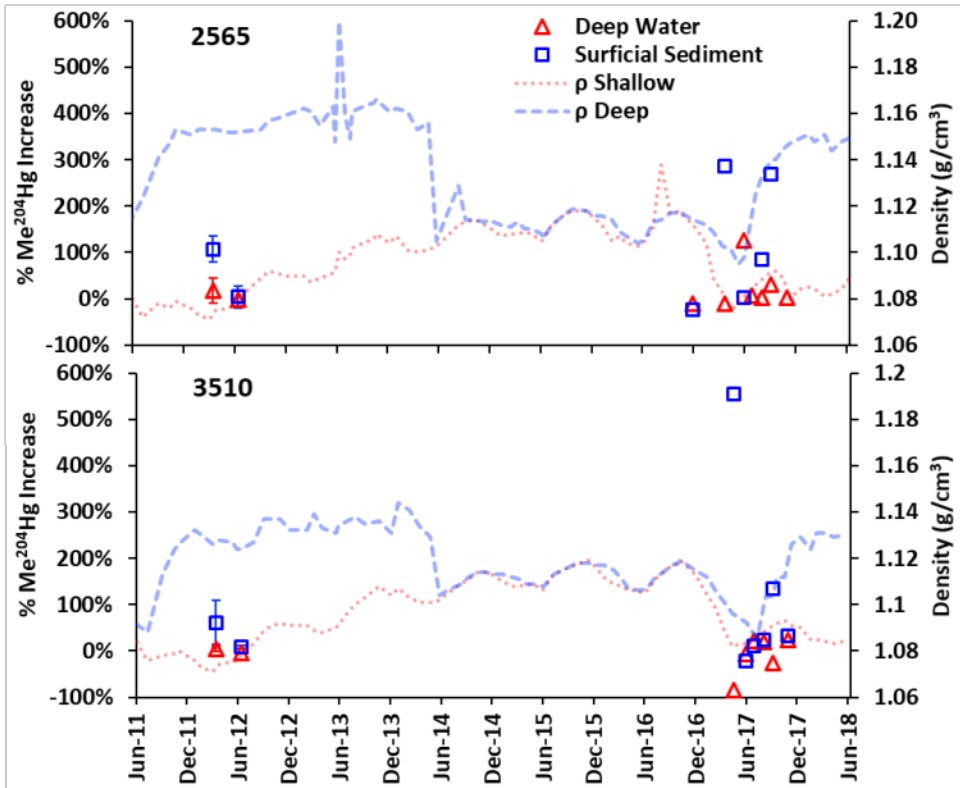


Figure A13. % of inorganic  $^{204}\text{Hg}$  spike that was methylated (% iHg spike methylated) during short-term incubation of deep waters and surficial sediment at sites 2565 and 3510 between 2010 and 2018 at sites. Density of shallow and deep waters are also displayed, but the desntiy scale is omitted for simplicity; see Figure 2.2.

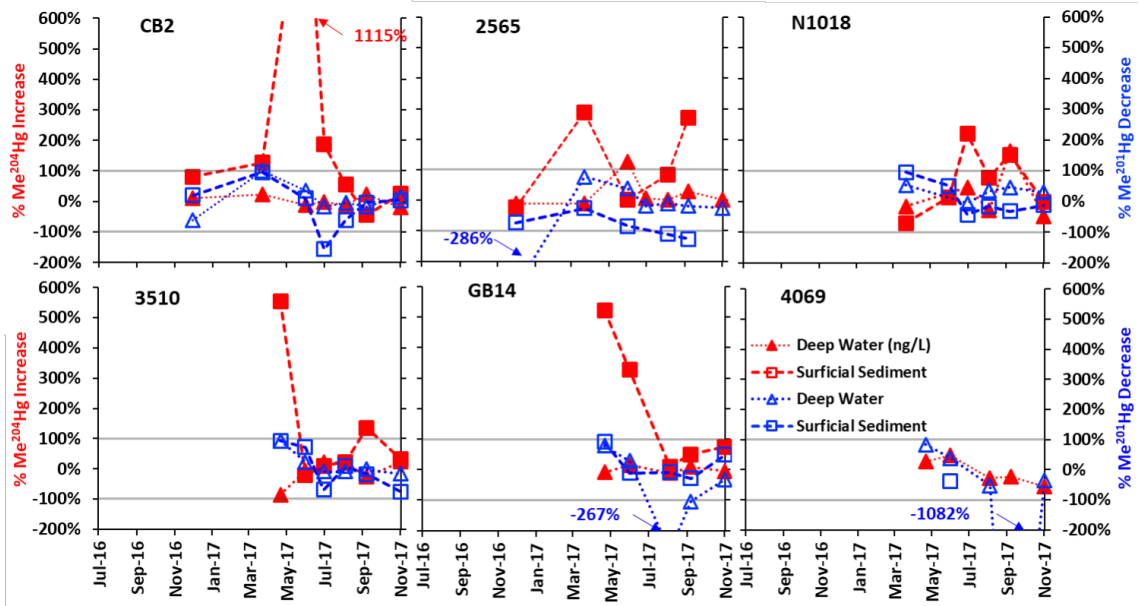


Figure A14. % Me<sup>204</sup>Hg increase (red solid symbols) and % Me<sup>201</sup>Hg decrease (blue open symbols) for deep water (triangles and dotted lines) and surficial sediments (squares and dashed lines) at six sites across the GSL. Horizontal lines represent the significant increase or decrease percentage (100% and -100%). Figure panels are ordered from northernmost site (CB2) to southernmost site (4069).

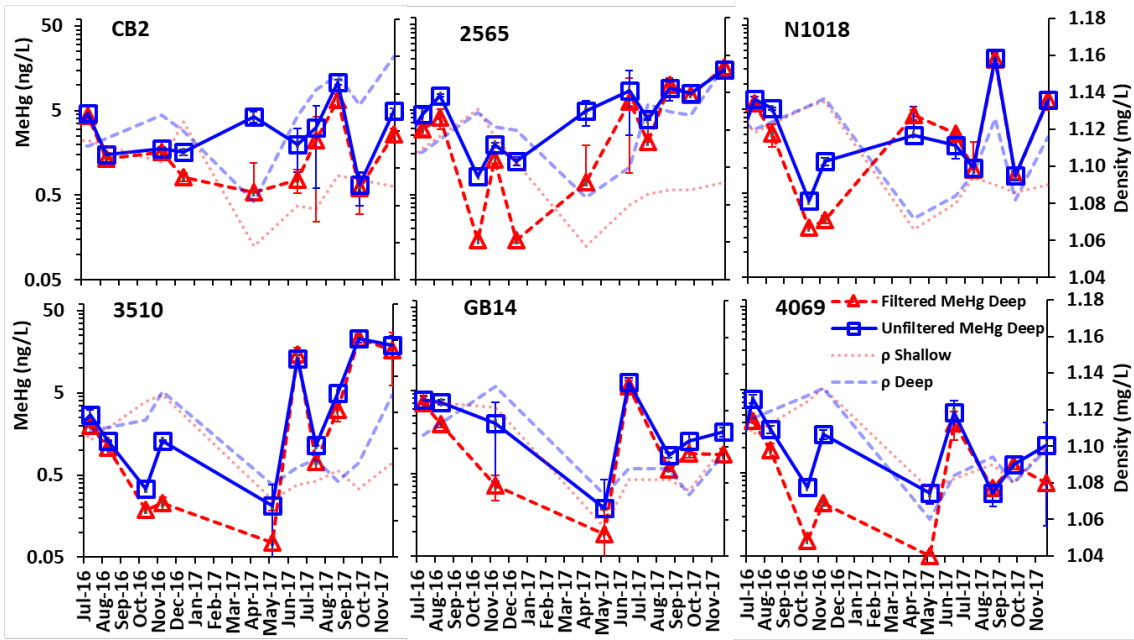


Figure A15. Deep water (0.5 m above bottom) unfiltered and filtered methyl mercury (MeHg) concentration and densities of shallow (0.2 m below water surface) and deep water at six sites across Great Salt Lake. Figure panels are ordered from northernmost site (CB2) to southernmost site (4069).

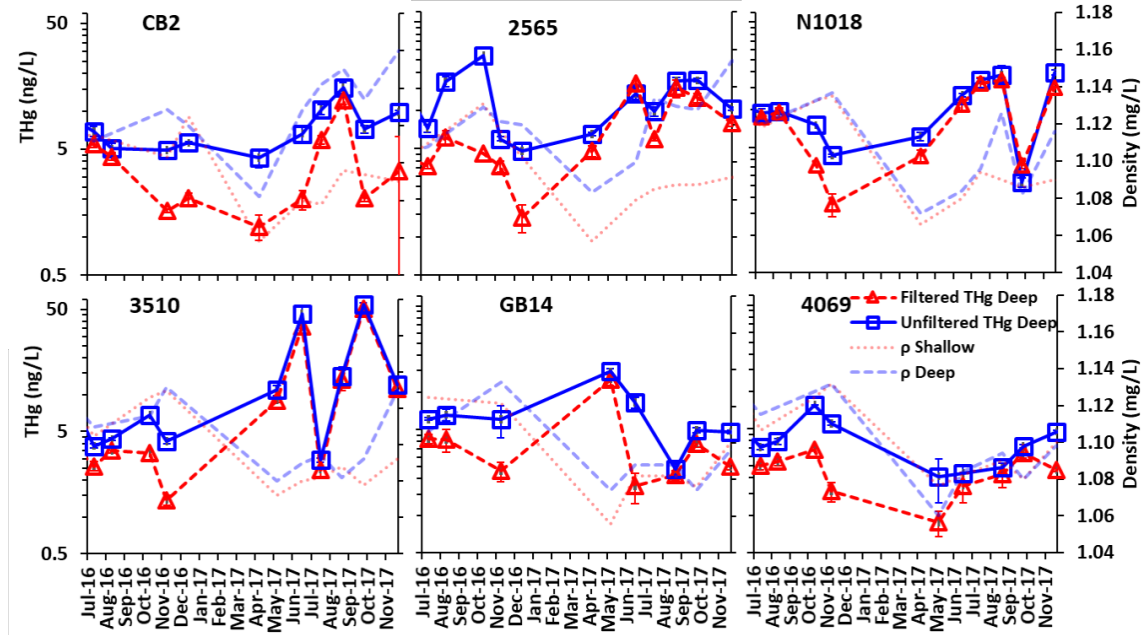


Figure A16. Deep water (0.5 m above bottom) unfiltered and filtered total mercury (THg) concentration and densities of shallow (0.2 m below water surface) and deep water at six sites across Great Salt Lake. Figure panels are ordered from northernmost site (CB2) to southernmost site (4069).

## **APPENDIX B**

### **SUPPORTING INFORMATION FOR CHAPTER 3**

Table B1: The matrix spike recovery rate for simulated Great Salt Lake water and Great Salt Lake brine samples.

	Simulated GSL water (Matrix spike recovery %)						GSL brine samples (Matrix spike recovery %)			
	Cu	Zn	Cd	As	Se	Pb	Cu	As	Se	Pb
1	102	110	73	75	74	82	107	83	56	61
2	105	110	75	76	70	72	109	84	58	59
3	102	103	82	79	78	87	112	91	66	61
4	105	111	79	72	67	77	127	97	70	62
5	102	103	85	73	76	88	-	-	-	-
6	102	100	87	75	73	83	-	-	-	-
<b>AVE</b>	103	106	80	75	73	81	114	89	63	61
<b>SD</b>	2	5	5	2	4	6	0.09	0.07	0.07	0.01

Table B2. % dissolved of trace elements in shallow and deep water

	Whole water column (%)		Shallow (%)		Deep (%)	
	AVE	SD	AVE	SD	AVE	SD
<b>Se</b>	95	24	94	23	96	26
<b>Cd</b>	97	20	99	24	95	15
<b>THg</b>	64	25	64	25	65	26
<b>Pb</b>	66	39	85	23	48	43
<b>Cr</b>	94	59	90	43	99	72
<b>As</b>	98	12	99	11	97	12
<b>Zn</b>	97	31	98	26	95	35
<b>Mo</b>	97	13	100	11	95	14
<b>Mn</b>	80	25	81	28	79	20
<b>U</b>	92	27	93	27	92	26
<b>Cu</b>	83	59	101	67	65	43
<b>MeHg</b>	60	37	48	27	73	41
<b>Fe</b>	54	42	66	47	41	31

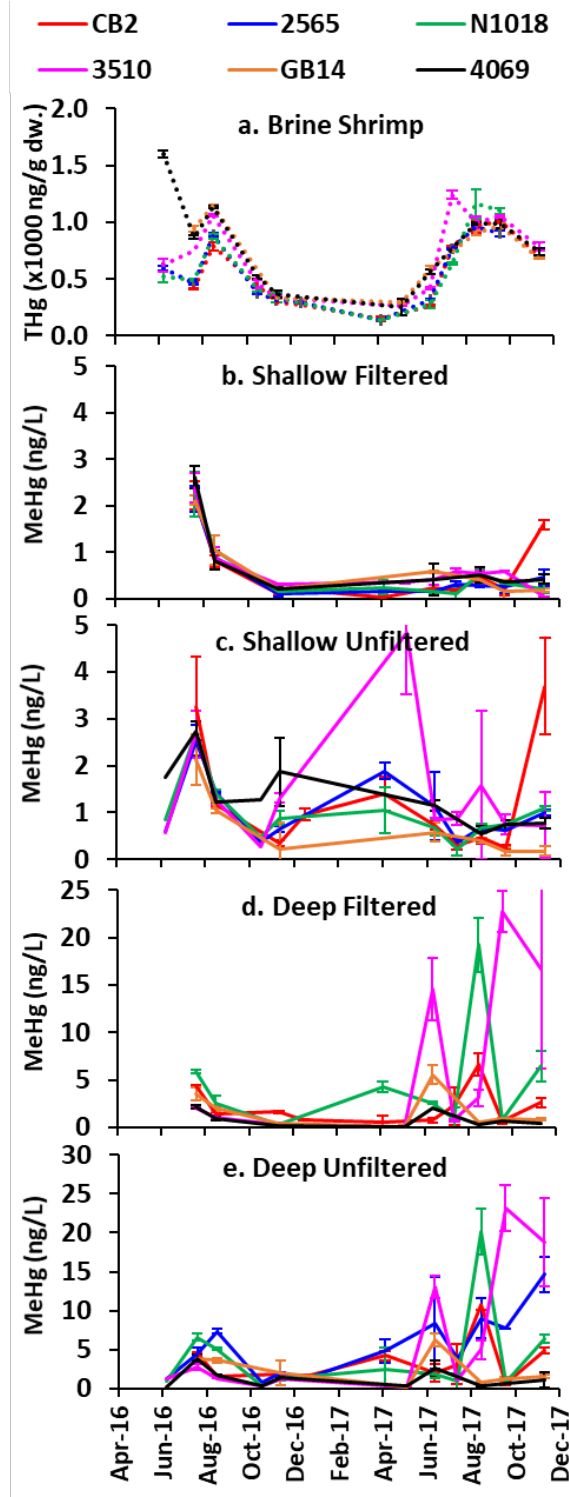


Figure B1. THg concentrations in a) brine shrimp, and MeHg concentrations in b) shallow filtered water, c) shallow unfiltered water, d) deep filtered water, and e) deep unfiltered water at six sites (denoted by color) across GSL. Dotted lines represent concentrations in brine shrimp, solid lines represent concentrations in water.

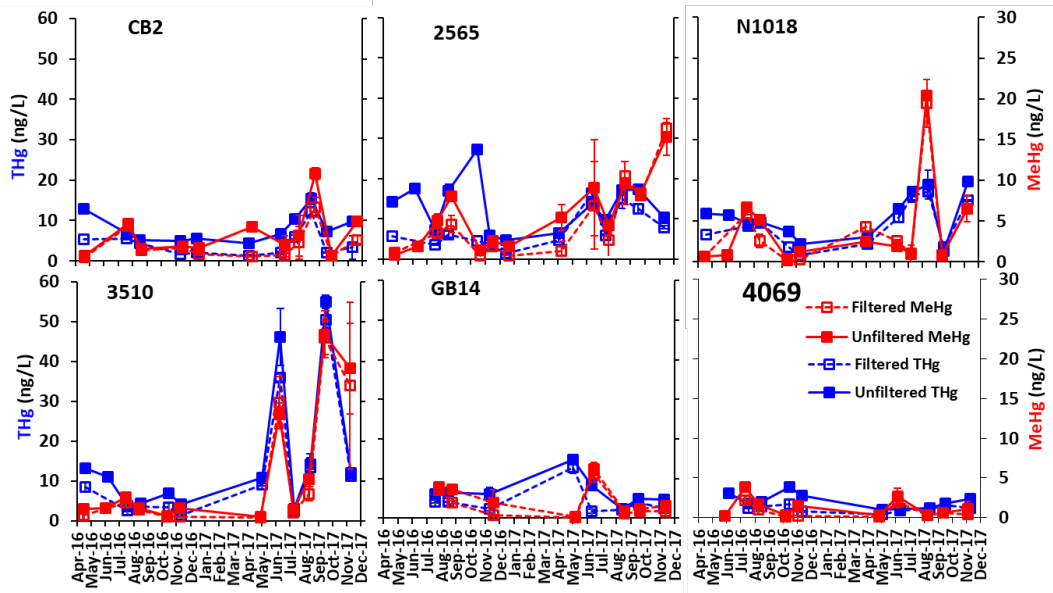


Figure B2. Filtered and unfiltered THg, MeHg, and sulfide concentrations in deep water at six sites. Figure panels are ordered northern sites in top row southern sites in bottom row.

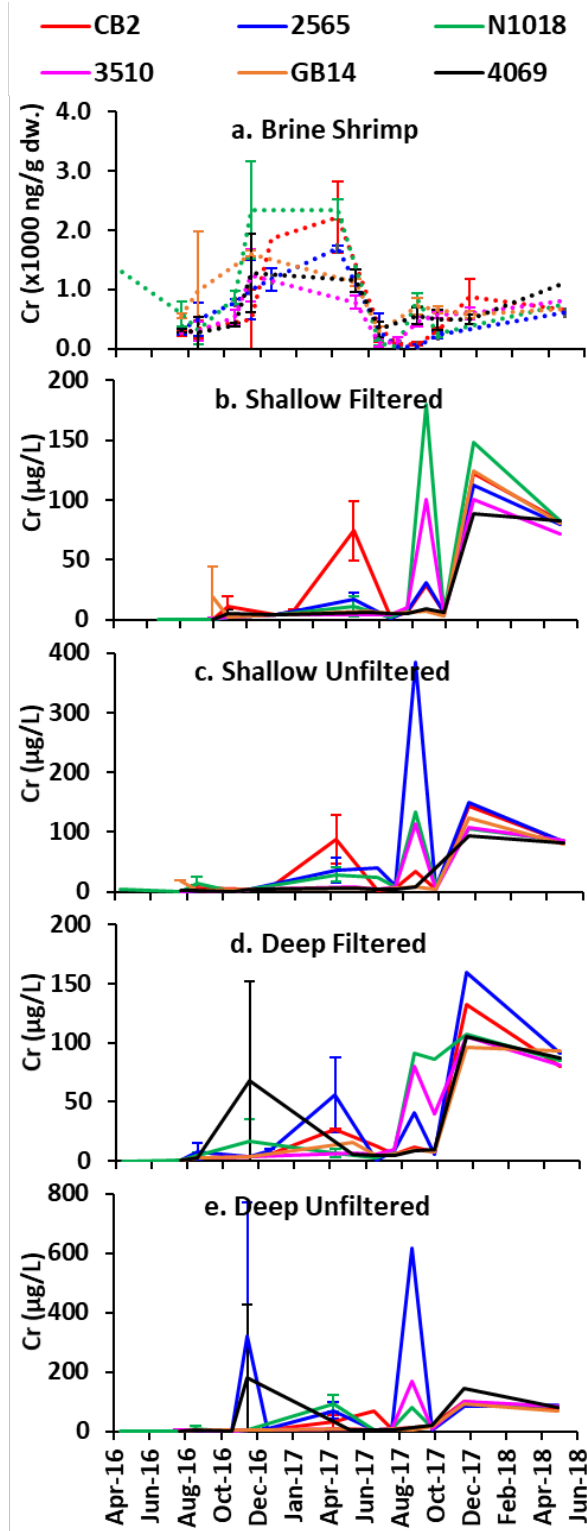


Figure B3. Cr concentrations in a) brine shrimp, b) shallow filtered water, c) shallow unfiltered water, d) deep filtered water, and e) deep unfiltered water at six sites (denoted by color) across GSL. Dotted lines represent concentrations in brine shrimp, solid lines represent concentrations in water.

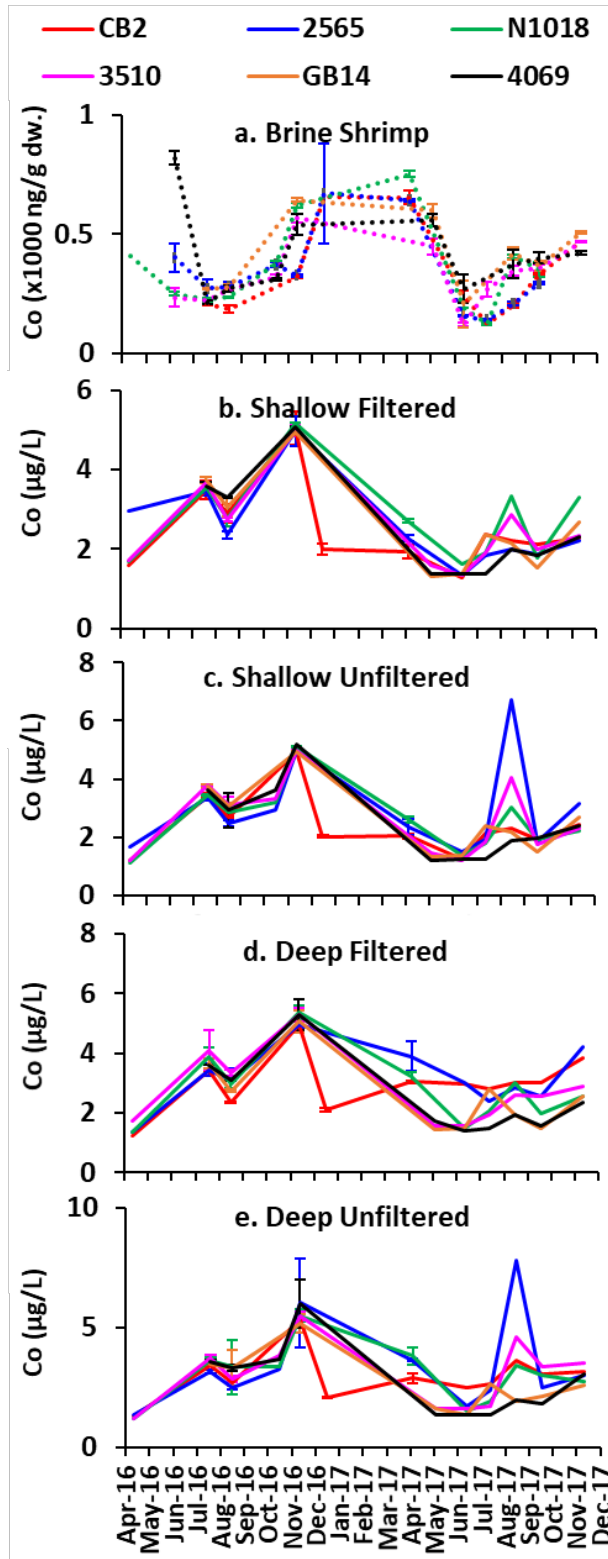


Figure B4. Co concentrations in a) brine shrimp, b) shallow filtered water, c) shallow unfiltered water, d) deep filtered water, and e) deep unfiltered water at six sites (denoted by color) across GSL. Dotted lines represent concentrations in brine shrimp, solid lines represent concentrations in water.

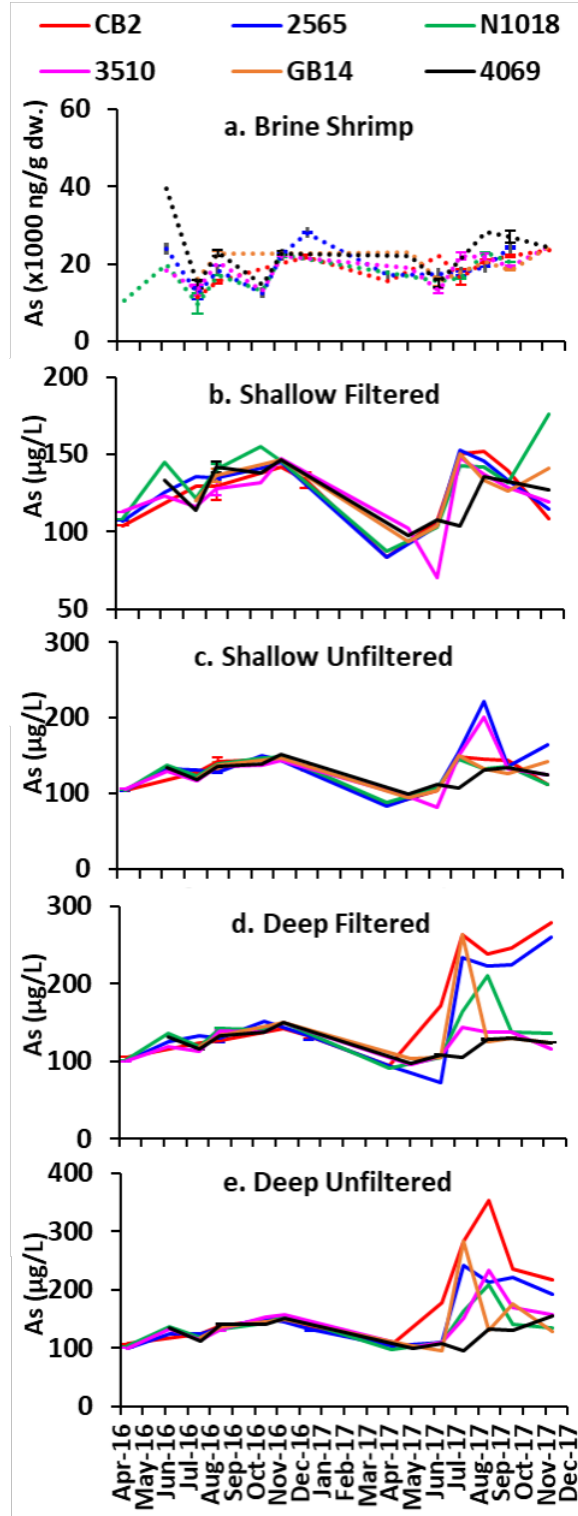


Figure B5. As concentrations in a) brine shrimp, b) shallow filtered water, c) shallow unfiltered water, d) deep filtered water, and e) deep unfiltered water at six sites (denoted by color) across GSL. Dotted lines represent concentrations in brine shrimp, solid lines represent concentrations in water.

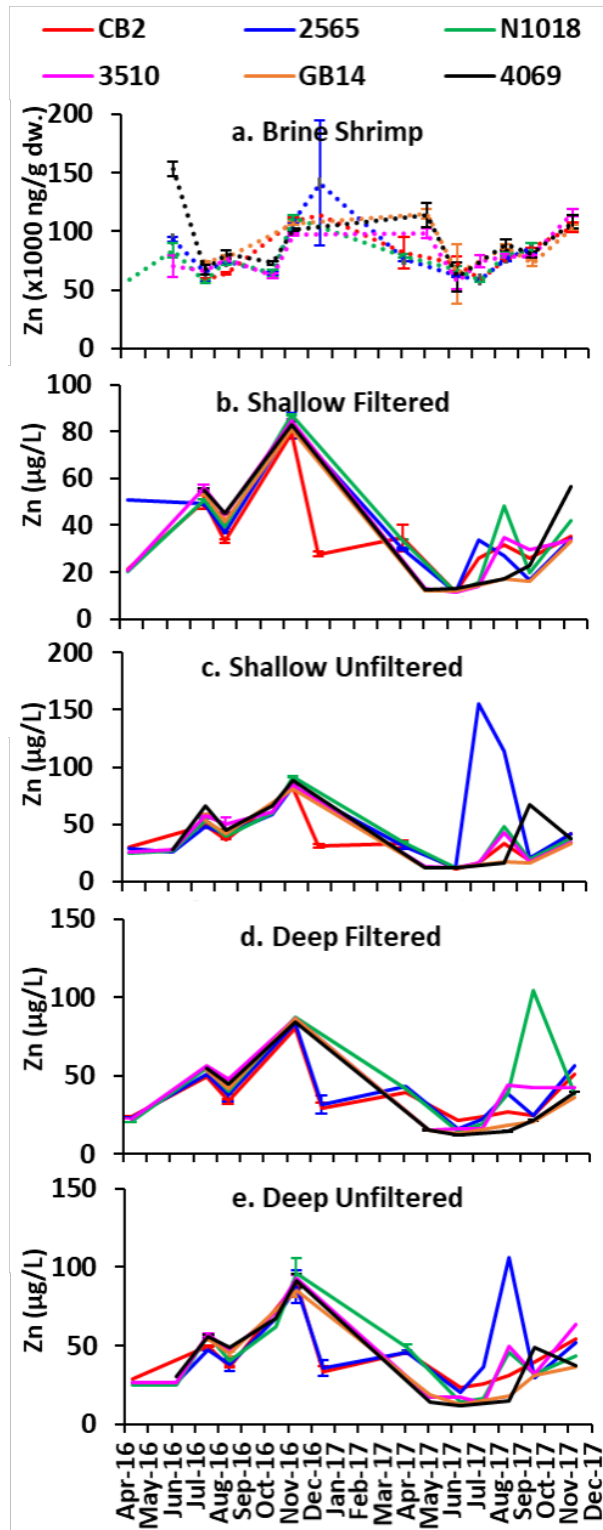


Figure B6. Zn concentrations in a) brine shrimp, b) shallow filtered water, c) shallow unfiltered water, d) deep filtered water, and e) deep unfiltered water at six sites (denoted by color) across GSL. Dotted lines represent concentrations in brine shrimp, solid lines represent concentrations in water.

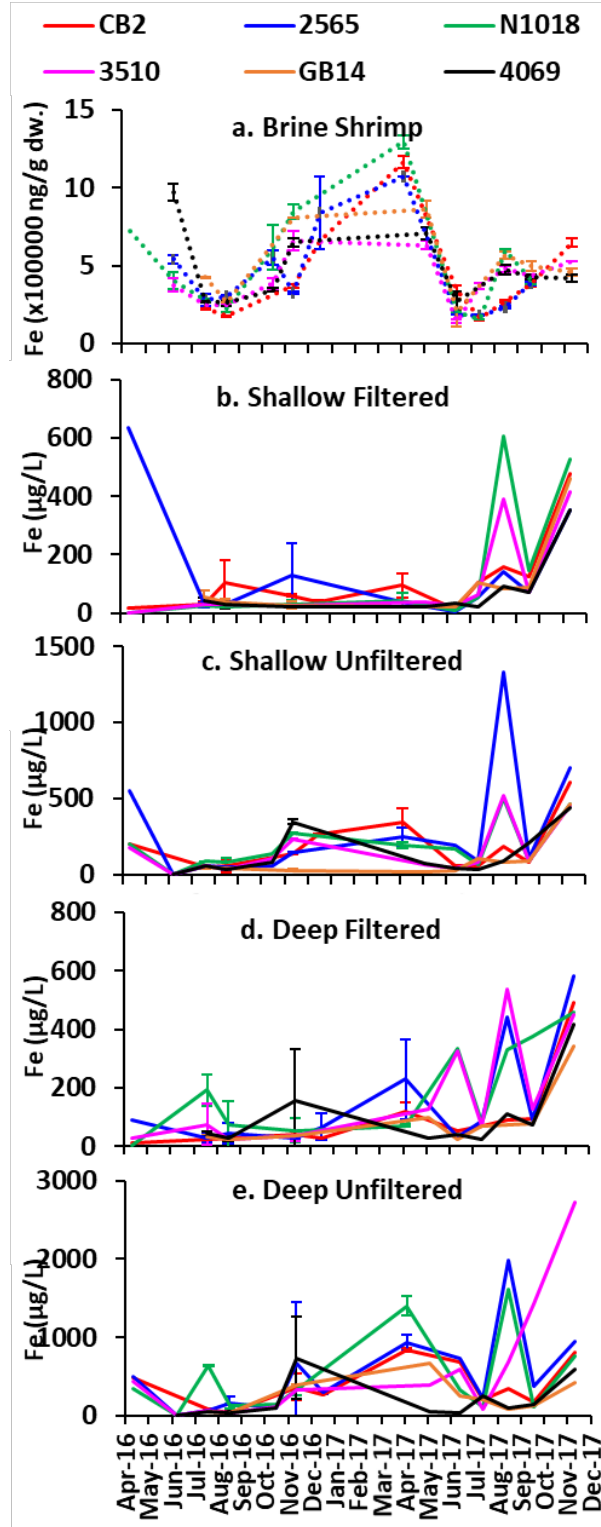


Figure B7. Fe concentrations in a) brine shrimp, b) shallow filtered water, c) shallow unfiltered water, d) deep filtered water, and e) deep unfiltered water at six sites (denoted by color) across GSL. Dotted lines represent concentrations in brine shrimp, solid lines represent concentrations in water.

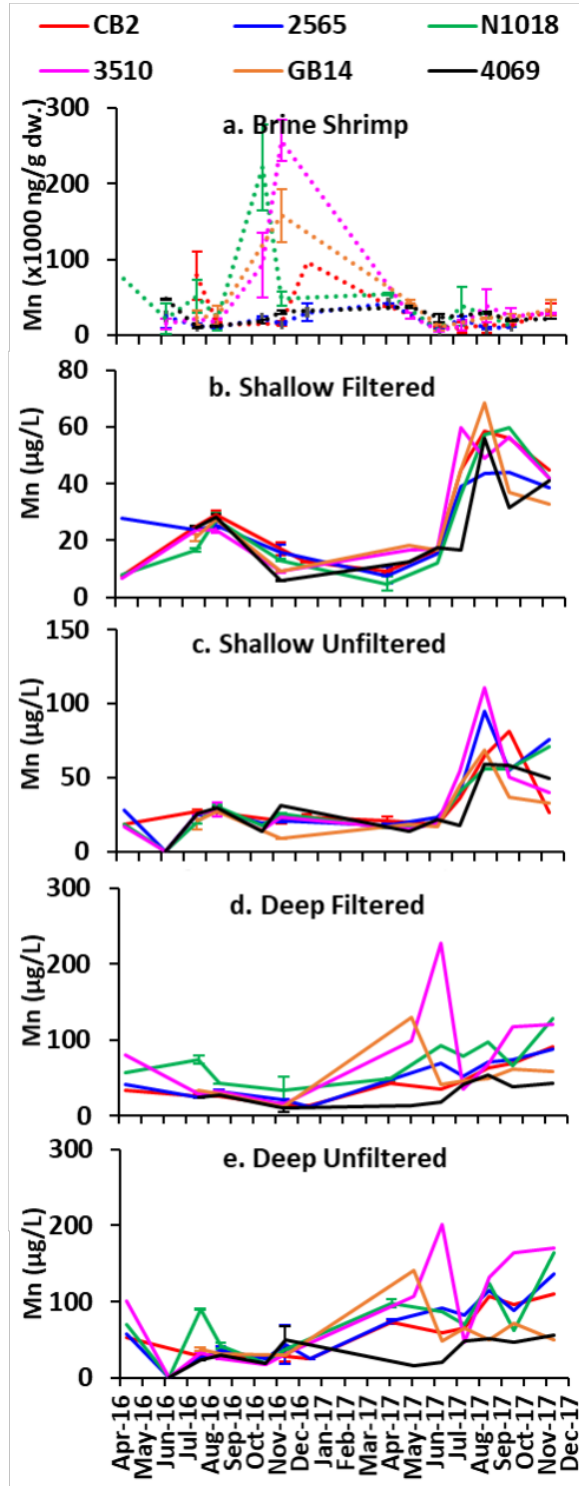


Figure B8. Mn concentrations in a) brine shrimp, b) shallow filtered water, c) shallow unfiltered water, d) deep filtered water, and e) deep unfiltered water at six sites (denoted by color) across GSL. Dotted lines represent concentrations in brine shrimp, solid lines represent concentrations in water.

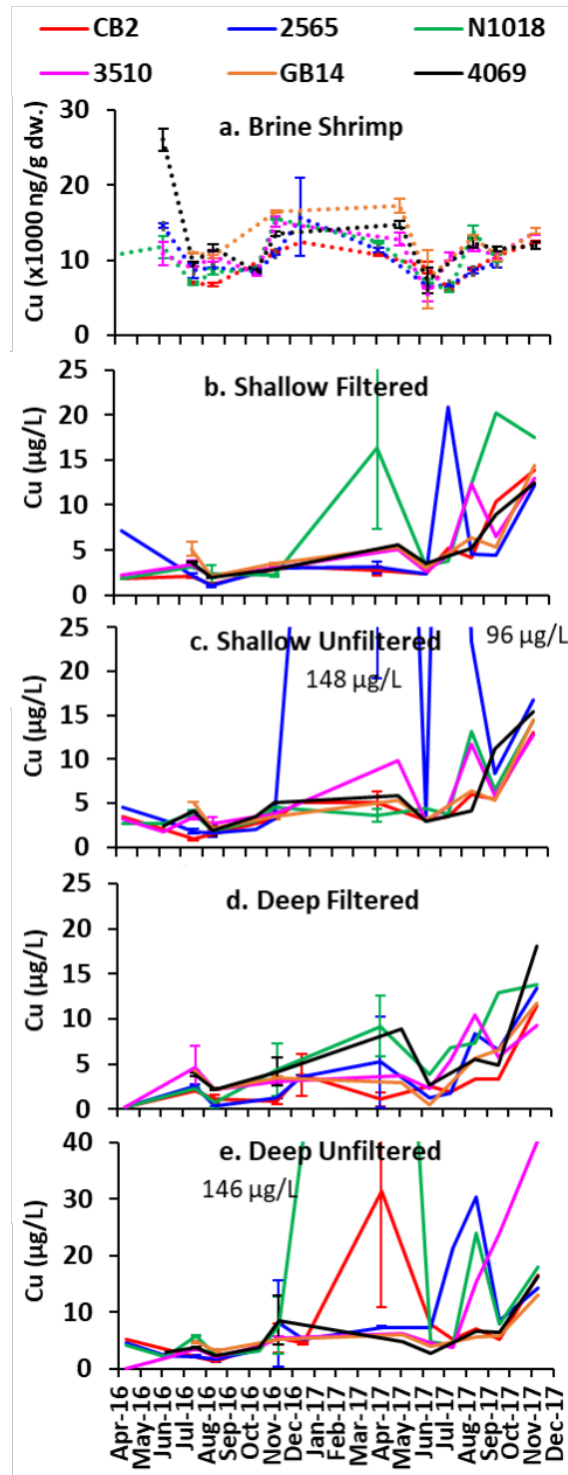


Figure B9. Cu concentrations in a) brine shrimp, b) shallow filtered water, c) shallow unfiltered water, d) deep filtered water, and e) deep unfiltered water at six sites (denoted by color) across GSL. Dotted lines represent concentrations in brine shrimp, solid lines represent concentrations in water. The highest value at 2565 in shallow unfiltered was 148  $\mu\text{g/L}$  in April 2017 and 96  $\mu\text{g/L}$  August 2017. The highest value at N1018 in deep unfiltered was 146  $\mu\text{g/L}$  in May 2017.

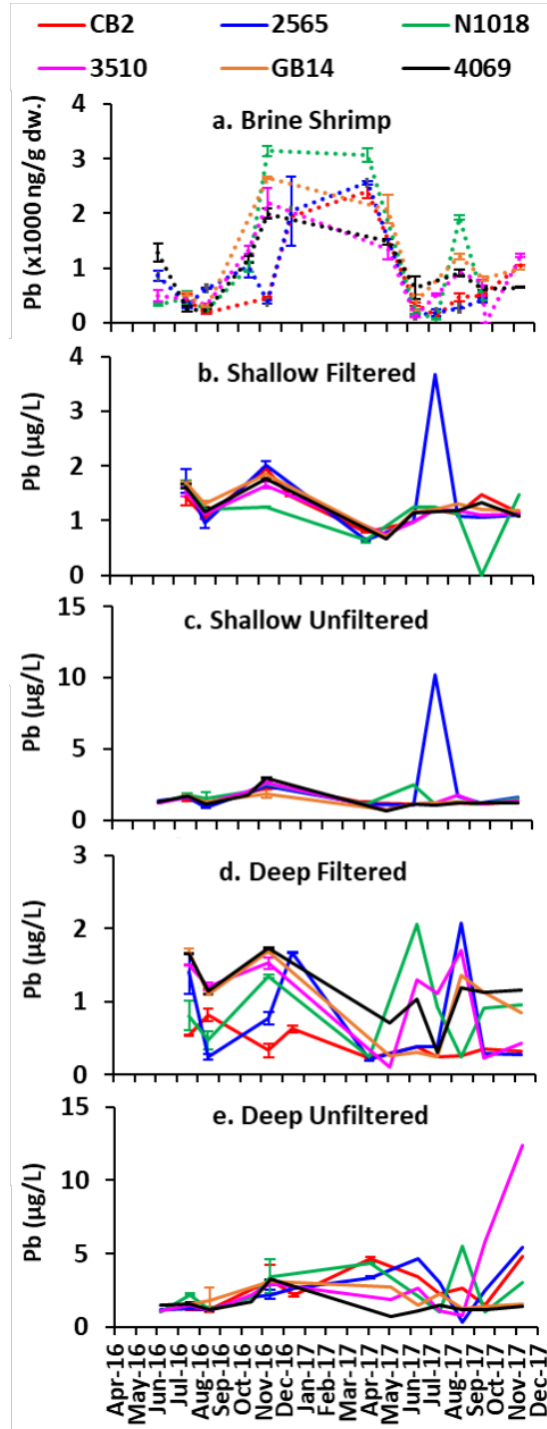


Figure B10. Pb concentrations in a) brine shrimp, b) shallow filtered water, c) shallow unfiltered water, d) deep filtered water, and e) deep unfiltered water at six sites (denoted by color) across GSL. Dotted lines represent concentrations in brine shrimp, solid lines represent concentrations in water.

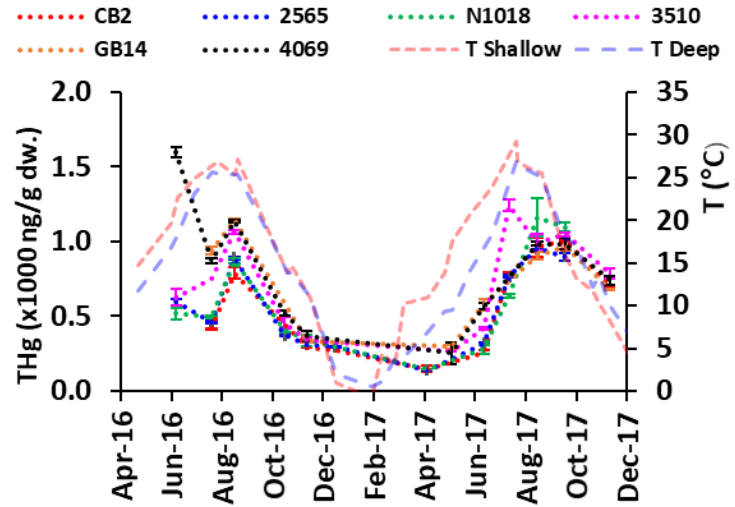


Figure B11. THg concentrations in water at six sites across the GSL, and water temperature in both shallow and deep water.

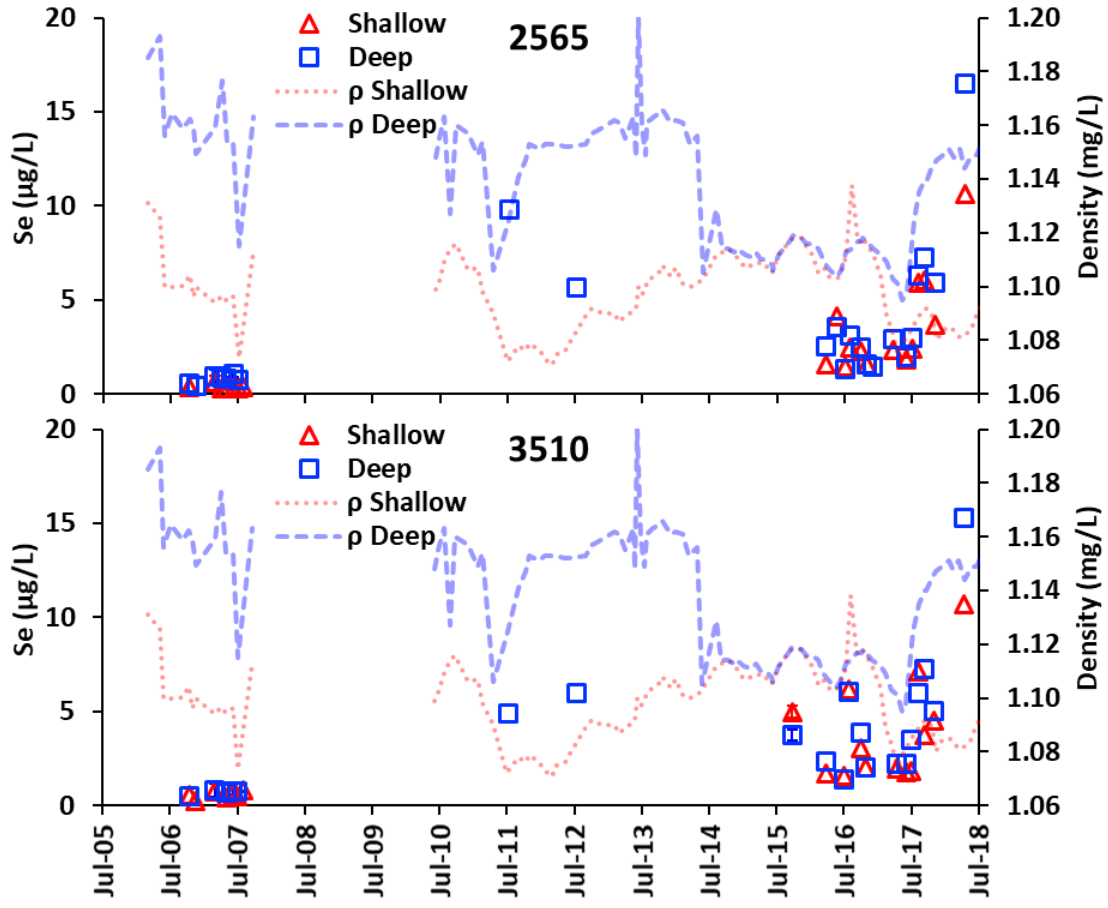


Figure B12. THg concentrations in water at six sites across the GSL, and water temperature in both shallow and deep water.

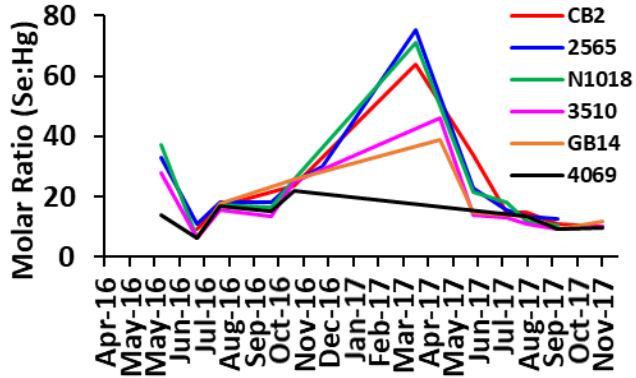


Figure B13. Molar ratio of Se to Hg concentrations in brine shrimp at six sites (denoted by color) across GSL.

## REFERENCES

- Ackerman, J.T., Herzog, M.P., Hartman, C.A., Isanhart, J.P., Herring, G., Vaughn, S., Cavitt, J.F., Eagles-Smith, C.A., Browers, H., Cline, C. and Vest, J., **2015**. Mercury and selenium contamination in waterbird eggs and risk to avian reproduction at Great Salt Lake, Utah (No. 2015-1020). US Geological Survey.
- Adams, W.J., DeForest, D.K., Tear, L.M., Payne, K. and Brix, K.V., **2015**. Long-term monitoring of arsenic, copper, selenium, and other elements in Great Salt Lake (Utah, USA) surface water, brine shrimp, and brine flies. *Environ. Monit. Assess.*, 187(3): 118-131.
- Aldrich, T.W. and Paul, D.S., **2002**. Avian ecology of Great Salt Lake. In: Gwynn, J.W. (Ed.), Great Salt Lake: An Overview of Change. Utah Department of Natural Resources Special Publication, 343-374.
- Amouroux, D. and Donard, O.F., **1996**. Maritime emission of selenium to the atmosphere in eastern Mediterranean seas. *Geophys. Res. Lett.*, 23:1777-1780.
- Arnon, A., Selker, J.S. and Lensky, N.G., **2016**. Thermohaline stratification and double diffusion diapycnal fluxes in the hypersaline Dead Sea. *Limnol. Oceanogr.*, 61:1214-1231.
- Beisner, K., Naftz, D.L., Johnson, W.P. and Diaz, X., **2009**. Selenium and trace element mobility affected by periodic displacement of stratification in the Great Salt Lake, Utah. *Sci. Total Environ.*, 407:5263-5273.
- Belovsky, G.E., Stephens, D., Perschon, C., Birdsey, P., Paul, D., Naftz, D., Baskin, R., Larson, C., Mellison, C., Luft, J. and Mosley, R., **2011**. The Great Salt Lake Ecosystem (Utah, USA): long term data and a structural equation approach. *Ecosphere*, 2:1-40.
- Black, F.J., Poulin, B.A. and Flegal, A.R., **2012**. Factors controlling the abiotic photo-degradation of monomethylmercury in surface waters. *Geochim. Cosmochim. Acta*, 84:492-507.
- Bloom, N.S., Colman, J.A. and Barber, L., **1997**. Artifact formation of methyl mercury during aqueous distillation and alternative techniques for the extraction of methyl mercury from environmental samples. *Fresenius J. Anal. Chem.*, 358:371–377.

- Brandt, K.K., Vester, F., Jensen, A.N. and Ingvorsen, K., **2001**. Sulfate reduction dynamics and enumeration of sulfate-reducing bacteria in hypersaline sediments of the Great Salt Lake (Utah, USA). *Microb. Ecol.*, 41:1-11.
- Brix, K.V., Deforest, D.K., Cardwell, R.D. and Adams, W.J., **2004**. Derivation of a chronic site-specific water quality standard for selenium in the Great Salt Lake, Utah, USA. *Environ. Toxicol. Chem.*, 23:606-612.
- Carling, G.T., Fernandez, D.P., Rudd, A., Pazmino, E. and Johnson, W.P., **2011**. Trace element diel variations and particulate pulses in perimeter freshwater wetlands of Great Salt Lake, Utah. *Chemical. Geology*, 283:87-98.
- Cline, C., Neill, J., Whitehead, J. and Gardberg, J., **2011**. Mercury concentrations in cinnamon teal (*Anas cyanoptera*) and northern shoveler (*Anas clypeata*) at Great Salt Lake, Utah., p. 130-150. In: Ecosystem Assessment of Mercury in the Great Salt Lake, Utah, 2008. Report for Department of Environmental Quality Division of Water Quality.
- Conover, M.R. and Vest, J.L., **2009**. Concentrations of selenium and mercury in eared grebes (*Podiceps nigricollis*) from Utah's Great Salt Lake, USA. *Environ. Toxicol. Chem.*, 28:1319-1323.
- Cordova, J.T. and Angeroth, C.E., **2012**. Runoff Conditions in Utah for Water Year 2011 (No. 2012-3041). US Geological Survey.
- DeForest, D.K., Brix, K.V. and Adams, W.J., **2007**. Assessing metal bioaccumulation in aquatic environments: the inverse relationship between bioaccumulation factors, trophic transfer factors and exposure concentration. *Aquat. Toxicol.*, 84:236-246.
- Diaz, X., Johnson, W.P. and Naftz, D.L., **2009**. Selenium mass balance in the Great Salt Lake, Utah. *Sci. Total Environ.*, 407:2333-2341.
- Diaz, X., Johnson, W.P., Fernandez, D. and Naftz, D.L., **2009**. Size and elemental distributions of nano- to micro-particulates in the geochemically-stratified Great Salt Lake. *Appl. Geochem.*, 24:1653-1665.
- Diaz, X., Johnson, W.P., Oliver, W.A. and Naftz, D.L., **2008**. Volatile selenium flux from the Great Salt Lake, Utah. *Environ. Sci. & Technol.*, 43:53-59.
- Dumont, H. J., **1998**. The Caspian Lake: history, biota, structure, and function. *Limnol. Oceanogr.*, 43: 44-52.
- Gwynn, J.W., **2002**. Great Salt Lake: chemical and physical variations of the brine and effects of the 2013SPRR causeway, 1966-1996. In: Gwynn, J.W. (Ed.), Great Salt Lake: An Overview of Change. Utah Department of Natural Resources Special Publication, 87-107.

- Hammerschmidt, C.R. and Fitzgerald, W.F., **2006**. Methylmercury in freshwater fish linked to atmospheric mercury deposition. *Environ. Sci. & Technol.*, 40:7764-7770.
- Harris, R.C., Rudd, J.W., Amyot, M., Babiarz, C.L., Beaty, K.G., Blanchfield, P.J., Bodaly, R.A., Branfireun, B.A., Gilmour, C.C., Graydon, J.A. and Heyes, A., **2007**. Whole-ecosystem study shows rapid fish-mercury response to changes in mercury deposition. *Proc. Natl. Acad. Sci. U.S.A.*, 104(42): 16586-16591.
- Hintelmann, H. and Evans, R.D., **1997**. Application of stable isotopes in environmental tracer studies—Measurement of monomethylmercury ( $\text{CH}_3\text{Hg}^+$ ) by isotope dilution ICP-MS and detection of species transformation. *Fresenius J Anal Chem.*, 358:378-385.
- Ingvorsen, K. and Brandt, K.K., **2002**. Anerobic microbiology and sulfur cycling in hypersaline sediments with special reference to Great Salt Lake. In: Gwynn J.W. (Ed.) Great Salt Lake: An Overview of Change. Utah Department of Natural Resources Special Publication. 387-398.
- Jewell, P., **2018**. Historic Low Stand of the Great Salt Lake, Utah: I. Mass Balance Model and Origin of the Deep Brine Layer, Submitted to Hydrology.
- Johnson, W.P., Swanson, N., Black, B., Rudd, A., Carling, G., Fernandez, D.P., Luft, J., Van Leeuwen, J. and Marvin-DiPasquale, M., **2015**. Total-and methyl-mercury concentrations and methylation rates across the freshwater to hypersaline continuum of the Great Salt Lake, Utah, USA. *Sci. Total Environ.*, 511:489-500.
- Jones, E. and Wurtsbaugh, W., **2014**. The Great Salt Lake's monimolimnion and its importance for mercury bioaccumulation in brine shrimp (*Artemia franciscana*). *Limnol. Oceanogr.*, 59:141-155.
- Loving, B.L., Miller, C.W. and Waddell, K.M., **2000**. Water and salt balance of Great Salt Lake, Utah, and simulation of water and salt movement through the causeway, 1987-98 (No. 2000-4221). US Geological Survey.
- Mason, R.P., Reinfelder, J.R. and Morel, F.M., **1996**. Uptake, toxicity, and trophic transfer of mercury in a coastal diatom. *Environ. Sci. & Technol.*, 30:1835-1845.
- Mergler, D., Anderson, H.A., Chan, L.H.M., Mahaffey, K.R., Murray, M., Sakamoto, M. and Stern, A.H., **2007**. Methylmercury exposure and health effects in humans: a worldwide concern. *Ambio*, 36: 3-11.
- Naftz, D., Angeroth, C., Kenney, T., Waddell, B., Darnall, N., Silva, S., Perschon, C. and Whitehead, J., **2008**. Anthropogenic influences on the input and biogeochemical cycling of nutrients and mercury in Great Salt Lake, Utah, USA. *Appl. Geochem.*, 23:1731-1744.

- Naftz, D., Angeroth, C., Kenney, T., Waddell, B., Darnall, N., Silva, S., Perschon, C. and Whitehead, J., **2008**. Anthropogenic influences on the input and biogeochemical cycling of nutrients and mercury in Great Salt Lake, Utah, USA. *Appl. Geochem.*, 23: 1731-1744.
- Naftz, D., Fuller, C., Cederberg, J., Krabbenhoft, D., Whitehead, J., Gardberg, J. and Beisner, K., **2009**. Mercury inputs to Great Salt Lake, Utah: reconnaissance-phase results. In: Oren, A. Naftz, D., Palacios, P. and Wurtsbaugh, W.A. (Eds.), Saline Lakes Around the World: Unique Systems with Unique Values. Natural Resources and Environmental Issues. S.J. and Jessie Quinney Natural Resources Research Library, 37-49.
- Ohlendorf, H.M., **2003**. Ecotoxicology of selenium. In: Hoffman, D.J., Rattner B.A., Burton G.A. Jr. and Cairns J. Jr. (Eds.), *Handbook of Ecotoxicology*. Lewis, Boca Raton, FL, USA, 465-500.
- Ohlendorf, H.M., DenBleyker, J., Moellmer, W.O. and Miller, T. **2009**. Development of a site-specific standard for selenium in open waters of Great Salt Lake, Utah. In: Oren, A., Naftz, D., Palacios, P. and Wurtsbaugh, W.A (Eds.), Saline Lakes around the World: Unique Systems with Unique Values. Natural Resources and Environmental Issues, Vol. 15, Article 4. pp. 23-36. S.J. and Jessie E. Quinney Natural Resources Research Library, Logan, UT.
- Orihel, D.M., Paterson, M.J., Blanchfield, P.J., Bodaly, R.A. and Hintelmann, H., **2007**. Experimental evidence of a linear relationship between inorganic mercury loading and methylmercury accumulation by aquatic biota. *Environ. Sci. & Technol.*, 41:4952-4958.
- Orihel, D.M., Paterson, M.J., Gilmour, C.C., Bodaly, R.A., Blanchfield, P.J., Hintelmann, H., Harris, R.C. and Rudd, J.W., **2006**. Effect of loading rate on the fate of mercury in littoral mesocosms. *Environ. Sci. & Technol.*, 40:5992-6000.
- Paterson, M.J., Blanchfield, P.J., Podemski, C., Hintelmann, H.H., Gilmour, C.C., Harris, R., Ogrinc, N., Rudd, J.W. and Sandilands, K.A., **2006**. Bioaccumulation of newly deposited mercury by fish and invertebrates: an enclosure study using stable mercury isotopes. *Can. J. Fish Aquat. Sci.*, 63:2213-2224.
- Pickhardt, P.C. and Fisher, N.S., **2007**. Accumulation of inorganic and methylmercury by freshwater phytoplankton in two contrasting water bodies. *Environ. Sci. & Technol.*, 41:125-131.
- Rueda, F. and Schladow, G., **2009**. Mixing and stratification in lakes of varying horizontal length scales: scaling arguments and energy partitioning. *L Limnol. Oceanogr.*, 54:2003-2017.
- Saxton, H.J., Goodman, J.R., Collins, J.N. and Black, F.J., **2013**. Maternal transfer of

- inorganic mercury and methylmercury in aquatic and terrestrial arthropods. *Environ. Toxicol. Chem.*, 32:2630-2636.
- Scheuhammer, A.M., Meyer, M.W., Sandheinrich, M.B. and Murray, M.W., **2007**. Effects of environmental methylmercury on the health of wild birds, mammals, and fish. *Ambio*. 36:12-8.
- Scholl, D.J. and Ball, R.W., **2005**. Utah Department of Health Office of Epidemiology Environmental Epidemiology Program, Salt Lake City, UT, USA.
- Scholl, D.J. and Ball, R.W., **2006**. Utah Department of Health Office of Epidemiology Environmental Epidemiology Program, Salt Lake City, UT, USA.
- Stephens, D.W., **1990**. Change in lake levels, salinity and the biological community of Great Salt Lake (Utah, USA), 1847-1987. *Hydrobiologia*, 197:139-46.
- USEPA Method 1630, **2001**. Methylmercury in Water by Distillation, Aqueous Ethylation, Purge and Trap, and CVAFS. U.S. Environmental Protection Agency.
- USEPA Method 1631, **2002**. (Appendix): Appendix to Method 1631: Total Mercury in Tissue, Sludge, Sediment, and Soil by Acid Digestion and BrCl Oxidation. U.S. Environmental Protection Agency.
- USEPA Method 1669, **1996**. Sampling Ambient Water for Trace Metals at EPA Water Quality Criteria Levels. U.S. Environmental Protection Agency.
- USEPA, **2000**. Guidance for assessing chemical contaminant data for use in fish advisories. 3rd ed, Fish Sampling and Analysis vol. 1. Publication No. EPA 823-B-00-007, Washington.
- Utah Division of Water Quality, **2014**. 2012-2014 Final Integrated Report Water Quality Assessment Program, Salt Lake City, UT, USA.
- Valdes, C., Black, F.J., Stringham, B., Collins, J.N., Goodman, J.R., Saxton, H.J., Mansfield, C.R., Schmidt, J.N., Yang, S. and Johnson, W.P., **2017**. Total mercury and methylmercury response in water, sediment, and biota to destratification of the Great Salt Lake, Utah, United States. *Environ. Sci. & Technol.*, 51:4887-4896.
- Vest, J.L., Conover, M.R., Perschon, C., Luft, J. and Hall, J.O., **2009**. Trace element concentrations in wintering waterfowl from the Great Salt Lake, Utah. *Arch. Environ. Contam. Toxicol.*, 56:302-316.
- Wang, W.X. and Wong, R.S., **2003**. Bioaccumulation kinetics and exposure pathways of inorganic mercury and methylmercury in a marine fish, the sweetlips Plectorhinchus gibbosus. *Mar. Ecol. Prog. Ser.*, 261:257-268.

- Watras, C.J. and Bloom, N.S., **1992**. Mercury and methylmercury, in individual zooplankton: implications for bioaccumulation. *Limnol. Oceanogr.*, 37:1313-1318.
- Wilhelm, S. and Adrian, R., **2008**. Impact of summer warming on the thermal characteristics of a polymictic lake and consequences for oxygen, nutrients and phytoplankton. *Freshwater Biol.*, 53:226-237.
- Wood, J.M., **1974**. Biological cycles for toxic elements in the environment. *Science*, 183: 1049-1052.
- Wurtsbaugh, W.A., Gardberg, J. and Izdepski, C., **2011**. Biostrome communities and mercury and selenium bioaccumulation in the Great Salt Lake (Utah, USA). *Sci. Total Environ.*, 409:4425-4434.
- Wurtsbaugh, W.A., Miller, C., Null, S.E., DeRose, R.J., Wilcock, P., Hahnberger, M., Howe, F. and Moore, J., **2017**. Decline of the world's saline lakes. *Nat. Geosci.*, 10:816-823.
- Yang, D.Y., Chen, Y.W., Gunn, J.M. and Belzile, N., **2008**. Selenium and mercury in organisms: interactions and mechanisms. *Environ. Rev.*, 16:71-92.
- Yang, S., Black, F.J. and Johnson, W.P., **2019**. Temporal correspondence and partitioning of selenium and mercury among brine shrimp and water in Great Salt Lake, Utah, USA (In preparation)
- Yang, S., Black, F.J., Johnson, W.P., Rowland, R., Rumsey, C. and Piskadlo, A., **2019**. Response of aquatic chemistry and methyl mercury concentrations in Great Salt Lake, Utah, USA to engineered and hydrologic forcings, *Limnol. Oceanogr.* (In submission)

ProQuest Number: 13882631

All rights reserved

INFORMATION TO ALL USERS

The quality of this reproduction is dependent on the quality of the copy submitted.

In the unlikely event that the author did not send a complete manuscript and there are missing pages, these will be noted. Also, if material had to be removed, a note will indicate the deletion.



ProQuest 13882631

Published by ProQuest LLC (2021). Copyright of the Dissertation is held by the Author.

All Rights Reserved.

This work is protected against unauthorized copying under Title 17, United States Code  
Microform Edition © ProQuest LLC.

ProQuest LLC  
789 East Eisenhower Parkway  
P.O. Box 1346  
Ann Arbor, MI 48106 - 1346